IOSR Journal of Pharmacy and Biological Sciences (IOSR-JPBS)
e-ISSN:2278-3008, p-ISSN:2319-7676. Volume 21, Issue 5 Ser. I (Sep. – Oct. 2026), PP 04-32
www.Iosrjournals.org

Quinoline-2-hydrazone Complexes of Co(II), Ni(II), Cu(II) and Zn(II): Coordination Features and Potential Antitubercular–Anticancer Activity

Laxmi A. Jagatap[1], Shivaraj S. Dolli[1], Ramesh Vadavi[1], Arun K Shettar[2], Joy H Hoskeri[3], Oruganti Anjaneyulu[4*], Kalagauda Gudasi[1,5**]

[1]Department of Chemistry, Karnatak University, Dharwad; [2]Division of Preclinical Research and Drug Development, Cytxon Biosolutions Pvt Ltd, Hubli; Department of Bioinformatics and Biotechnology, Karnataka State Akkamahadevi Women University, Vijayapura; [4]Department of Chemistry, Central University of Karnataka, Kalaburgi; [5]Sri Jagadguru Murugharajendra University, Chitradurga
***Corresponding Author:** Oruganti Anjaneyulu*
****Corresponding Author:** Kalagauda Gudasi*

Abstract:
The synthesis of quinoline-based hydrazones was carried out using common organic solvents and followed by their complexation with Co(II), Ni(II), Cu(II), and Zn(II) salts, which were characterised by various analytical techniques such as NMR (^{1}H and ^{13}C), ESI-MS, FTIR, TGA, UV-Visible, and the molecular structure of ligand L3 was unambiguously established by single-crystal X-ray diffraction. The compounds were evaluated for anti-tubercular activity against Mycobacterium tuberculosis in Middlebrook 7H9 medium using the microplate Alamar Blue assay (MABA); moderate activity was observed. The ligands and their copper complexes were evaluated for anticancer activity against MDA-MB-231, a breast cancer cell line, and IC_{50} values indicate that the copper complexes show greater activity than the ligands alone, with a clear decrease; most IC_{50} values of the tested samples are less than 25µg/mL. These findings demonstrate the potential of quinoline-based hydrazone metal complexes as promising candidates for further investigation as antitubercular and anticancer agents.

Keywords: *Quinoline hydrazone, heterocyclic ligand, Copper(II) complex, Anti-tubercular activity, Breast cancer.*

Date of Submission: 03-09-2026 Date of Acceptance: 13-09-2026

Graphical Abstract:

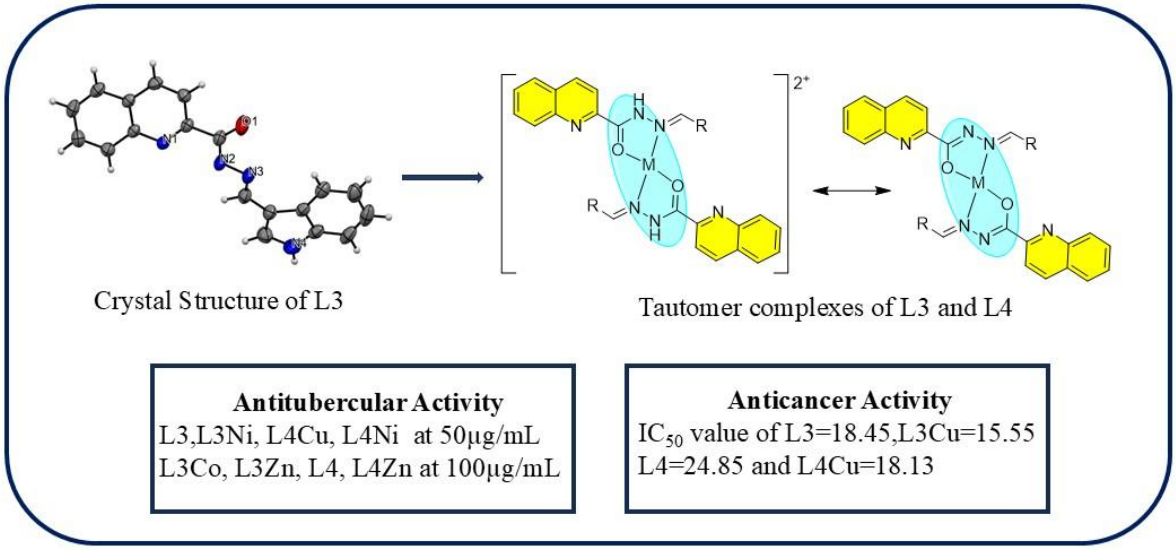

I. Introduction:

Tuberculosis (TB) and breast cancer remain major global health challenges. The treatment of TB has become increasingly difficult because of the emergence of drug-resistant strains, treatment-related toxicity, and the limited availability of effective therapeutic options. According to reports from the World Health Organization,

continued research and development of new antitubercular drugs are essential for overcoming drug resistance and achieving the objectives of the End TB Strategy.[1] Despite ongoing progress in diagnostics, drug pipelines, and drug development, current options are insufficient to overcome rising drug resistance and meet End TB Strategy goals and cure the deadly disease, breast cancer[2]. Sustained investment and innovation are essential to accelerate the development of more effective treatments and to design new medicines.

Schiff base metal complexes are widely recognized in the literature and have been investigated for a wide range of applications, such as antibacterial[3, 4], anticancer[5], and antimalarial[6] antitubercular properties, including their significance in photochemistry and molecular sensing. Their multifunctional uses, ease of synthesis, superior solubility in common organic solvents, and the presence of anharmonic protons—a feature shared by hydrazone derivatives—all contribute to their widespread interest and enable them to form chelate complexes with many metal salts[7, 8]. Because of their versatile coordination behavior, these hydrazones can coordinate to metal ions in both bidentate and tridentate modes, greatly increasing the stability of the resulting metal complexes[9].

The Quinoline bearing hydrazones have been extensively investigated because of the diverse pharmacological properties associated with both the quinoline and hydrazone moieties. Several quinoline-based hydrazones have demonstrated promising antitubercular and anticancer [10, 11] especially those compounds that include a carbonyl group adjacent to the hydrazone moiety, and even the 2 substituted quinoline molecules exhibit good bioactivity as well as fluorescent properties of interest to photo-chemists and have also gained interest in fingerprint detection research[12]which explores new doors for forensic studies.

Looking onto the versatile applications and the research gap generated we designed 2-quinoline carboxylic based hydrazones with indole-3-carbaldehydehyde and 4-florobenzaldehyde which also tested to exhibit antitubercular and good anticancer properties and both the ligands were synthesized without any column chromatography and led to complexation with Cu(II), Co(II), Ni(II) and Zn(II) metal ions and these were analysed by various analytical techniques, after confirmation these compounds we subjected to anti-tubercular activity against M. tuberculosis and the ligands and their Cu(II) complexes for anticancer activity against the triple negative breast cancer cell line MDAMB-231 using MTT based cell viability assay.

II. EXPERIMENTAL SECTION:

Materials and Methods

Reagents and Instruments: Most of the chemicals are from SD Fine and Spectrochem, with some solvents from Molychem. All the chemicals were directly used without any further purification process, and the solvents used were recovered and reused during the isolation of the compounds to be in line with greener chemistry. All reactions were monitored by thin-layer chromatography (TLC), and preparative TLC was performed with silica gel plates using silica gel 60 GF254 (Merck Life Science Private Ltd, USA). Melting points were determined in an open capillary using a WRS-2U melting point apparatus and were uncorrected. The IR spectra were obtained using a Nicolet 6700 FT-IR spectrometer. In DMSO-d_6, and $CDCl_3$, NMR (^1H and ^{13}C), spectra were collected using a Jeol 400 MHz FTNMR spectrometer. Mass spectra were recorded using a Waters-USA Xevo G2-XS Q-TOF mass spectrometer. The IR spectra were recorded in the 4000–400 cm^{-1} region on a Nicolet 170 SX FT-IR spectrometer using KBr discs. A Jasco-P-670 UV–Visible spectrophotometer was used to collect electronic spectra in the 200–800 nm range. The Hitachi F-7000 Fluorescence Spectrophotometer was used to measure the fluorescence spectra. A super Nova X-ray diffractometer was used to collect intensity data, and direct methods were used to solve the structure, followed by full-matrix least-squares refinement of F2 using the SHELXTL program. Thermal studies were carried out on a TGA7 ANALYSER, Perkin–Elmer, US, in the temperature range 27–800°C with a heating rate of 10°C per min.

Synthesis of ligand L3 and L4:

Quinolinic acid (0.1 M) 1 was dissolved in 30 mL of dry methanol, to which 1 mL of sulfuric acid was added, and the mixture was refluxed for about 16 hours to obtain **2**, a methyl ester. 0.1 M of ***2*** was treated with 0.5 M hydrazine hydrate and was refluxed in a methanolic solution for about 10 hours. The precipitate obtained ***3,*** was vacuum-filtered, washed with cold ethanol, dried, and used without further purification due to its moisture-sensitive nature (i.e., it would change colour to brown). 0.1 M of ***3*** was treated with 0.12 M of indole-3-carbaldehyde and was stirred at room temperature in Dry methanol as a solvent, and a catalytic amount of Glacial Acetic acid was added to the reaction mixture. The reaction progress was monitored under TLC. A lemon-yellow precipitate was obtained, which was filtered and washed with ethanol and methanol. And then recrystallized using methanol and propanol (3:1 ratio), the solid obtained was dried to obtain **L3**[13]. **[Scheme 1]** (Yield -70%) Melting point 186-190°C. Colour and nature of the ligand – lemon yellow colour precipitate crystalline after recrystallization.^1H NMR of L3 (400 MHz, DMSO-D_6) δ 11.88 (s, 1H), 11.62 (d, J = 2.7 Hz, 1H), 8.83 (s, 1H), 8.58 (d, J = 8.5 Hz, 1H), 8.35 – 8.27 (m, 1H), 8.19 (dd, J = 8.4, 2.6 Hz, 2H), 8.07 (dd, J = 8.3, 1.4 Hz, 1H), 7.87 (ddd, J = 8.4, 6.8, 1.5 Hz, 1H), 7.81 (d, J = 2.7 Hz, 1H), 7.71 (ddd, J = 8.1, 6.8, 1.2 Hz, 1H), 7.46 – 7.39 (m, 1H), 7.17 (dtd, J = 16.5, 7.1, 1.4 Hz, 2H). Similarly, ***3*** was treated with 4-fluorobenzaldehyde to obtain **L4.** (Yield -75%) Melting point

78-82℃. Colour and nature of the ligand – colourless crystalline after recrystallization.[1]H NMR of **L4** (400 MHz, $CDCl_3$) δ 11.20 (d, *J* = 7.6 Hz, 1H), 8.38 (dt, *J* = 17.2, 8.2 Hz, 3H), 8.12 (d, *J* = 8.3 Hz, 1H), 7.93 – 7.72 (m, 4H), 7.64 (t, *J* = 7.6 Hz, 1H), 7.11 (t, *J* = 8.5 Hz, 2H).

Scheme

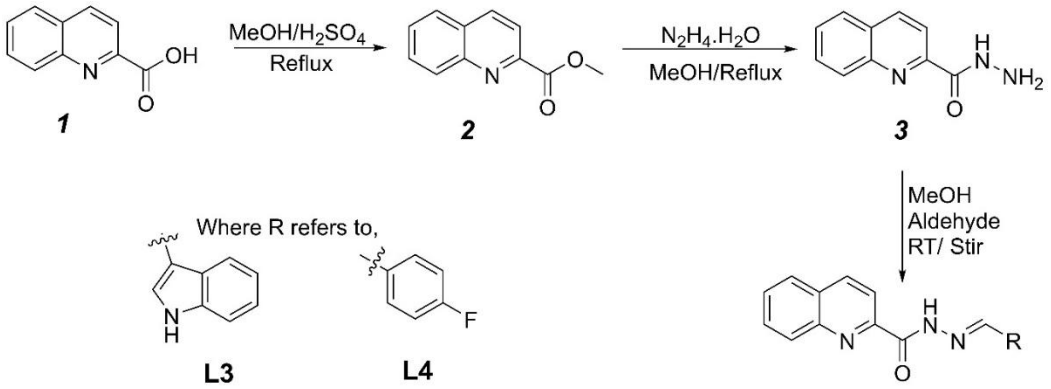

Synthesis of Complexes

0.5 mmol of metal chloride was dissolved in a minimum (3ml) of methanol, added to the 0.5 mmol of L3 dissolved in hot methanol, and stirred at room temperature. An immediate color change was observed, which gradually precipitated at different time intervals for different metals. The obtained solids were filtered and washed with methanol and ethanol. The obtained filtrate was reduced and kept for crystallization. Cu(II) and Zn(II) complexes precipitated immediately within a few minutes, but the Co(II) and Ni(II) complexes took around 5-8 hours to precipitate. Yielding 60-85%, the melting point of the metal complexes exceeded 250℃. Similarly, L4 Complexes were prepared. Yielding 70-85%, the melting point of the metal complexes exceeded 250℃. [1]H NMR of L3Zn (600 MHz, DMSO) δ 12.22 (s, 2H), 8.91 (d, *J* = 8.5 Hz, 2H), 8.74 (s, 2H), 8.63 3(d, *J* = 8.4 Hz, 2H), 8.53 – 8.40 (m, 4H), 8.32 (s, 3H), 8.28 – 8.20 (m, 6H), 8.13 (dd, *J* = 8.2, 1.4 Hz, 2H), 8.06 (t, *J* = 7.7 Hz, 2H), 7.92 (ddd, *J* = 8.3, 6.8, 1.5 Hz, 3H), 7.84 (qd, *J* = 5.6, 2.2 Hz, 8H), 7.76 (ddd, *J* = 8.1, 6.7, 1.2 Hz, 2H), 7.31 (dt, *J* = 29.8, 8.7 Hz, 8H).[1]H NMR of L4Zn - (600 MHz, DMSO) δ 11.80 (s, 1H), 11.55 (d, *J* = 2.8 Hz, 1H), 8.90 – 8.86 (m, 1H), 8.78 (s, 1H), 8.53 (d, *J* = 8.5 Hz, 1H), 8.24 (dd, *J* = 33.8, 9.7 Hz, 2H), 8.14 (dd, *J* = 8.4, 2.8 Hz, 3H), 8.03 (dd, *J* = 8.2, 1.5 Hz, 2H), 7.83 (ddd, *J* = 8.3, 6.8, 1.5 Hz, 2H), 7.76 (d, *J* = 2.7 Hz, 1H), 7.66 (ddd, *J* = 8.1, 6.6, 1.1 Hz, 1H), 7.47 (d, *J* = 6.3 Hz, 1H), 7.38 (d, *J* = 8.0 Hz, 1H), 7.21 – 7.08 (m, 4H).

Results and Discussions

ESI mass studies

The molecular ion peak of L3 observed with an m/z value resonating at 315(M+1) corresponds to the molecular weight of the ligand. The ESI-MS spectra of Co(II), Ni(II), Cu(II) and Zn(II) complexes of L3 show molecular ion peaks with m/z values at 686[M-$(Cl^-)_2$]$^{2+}$], 686[M-$(Cl^-)_2$]$^{2+}$, 798 (M+1), and 798[M+1] corresponding to the molecular weight of the complexes in $[ML_2]Cl_2$ type of the complexes for Co(II), Ni(II): whereas, $ML_2Cl_2.2H_2O$ for Cu(II) and Zn(II)[14, 15]. These values are in good agreement with the proposed composition for the complexes. The molecular ion peak of L4 was observed with an m/z value resonating at 292(M+1), corresponding to the molecular weight of the Ligand. ESI-MS spectra of Co(II), Ni(II), Cu(II) and Zn(II) complexes of L4 show molecular ion peaks with m/z values at 644(M+1), 643(M+), 649(M+1), 649 [M-$2Cl^-$]$^{2+}$. Hence, the mass studies confirm the formation of the complexes in the expected ratio. The ESI- MS plots are given in **Fig.S18- S28**.

Infrared spectral studies

The diagnostic FTIR spectral bands of ligands and their metal complexes are presented in Table 1 and 2. The ligand L3 has 2 characteristic NH stretching frequencies at 3298 cm^{-1} and 3169 cm^{-1}, which, due to tautomerisation in copper(II), and zinc(II) complexes, we can only observe a single indole NH stretching frequency, which is weak. In contrast, in cobalt(II) and nickel(II) complexes, we observe both the NH stretching frequencies, which indicates no tautomerisation occurred, and there is also no carbonyl stretching frequency, which supports the absence of NH stretching frequencies for copper(II) and zinc(II) complexes[16]. The FTIR spectral data of L4 has been observed to have a sharp NH stretching frequency at 3251 cm^{-1} and a carbonyl stretching frequency at 1673 cm^{-1}. The NH stretching frequencies and carbonyl stretching frequency for all Co(II), Cu(II), and Ni(II) complexes of ligand L4 are absent, which suggests that tautomerisation has occurred for all the complexes. For the Zn(II) complex, tautomerisation did not occur, as the NH stretching frequency was found around 3234 cm^{-1}. The FTIR plots of all the compounds are given in **Fig. S1-S10**.

Table 1 FTIR Results of L3, L3Co, L3Cu, L3Ni, and L3Zn

Sample ID	ν(NH) hydrazone (cm^{-1})	ν(NH) indole ring (cm^{-1})	ν(C=O) (cm^{-1})	ν(C=N) Hydrazone (cm^{-1})	ν(C-O)/ ν(C-N) (cm^{-1})	ν(C=N) Quinoline (cm^{-1})	ν(M-O) (cm^{-1})
L3	3298(s)	3169 (br,w)	1673	1537	1242	1610	-
L3Co	3252(s)	3156(w)	1643	1559	1230	1610	509
L3Cu	-	3056(w)	-	1542	1230/1129	1609	490
L3Ni	3236(s)	3166(w)	1647	1560	1254	1611	463
L3Zn	-	3149(w)	-	1551	1224/1126	1581	491

Table 2 FTIR Results of L4, L4Co, L4Cu, L4Ni, and L4Zn

Sample ID	ν(NH) (cm^{-1})	ν(C=O) (cm^{-1})	ν(C=N) Hydrazone (cm^{-1})	ν(C-O) /ν(C-N) (cm^{-1})	ν(C=N) Quinoline (cm^{-1})	ν(M-O) (cm^{-1})
L4	3251	1691	1541	1228	1599	-
L4Co	-	-	1561	1235/1160	1606	485
L4Cu	-	-	1539	1234/1554	1597	494
L4Ni	-	-	1563	1235/1160	1607	524
L4Zn	3234	1637	1557	1224	1600	526

NMR Studies:

In the ^{1}H NMR spectrum of the ligand L3, the indole NH proton resonates at 11.9 ppm, the hydrazide (C=O-NH) proton at 11.7 ppm, and the azomethine proton at 8.9 ppm, aromatic protons are in the range 7.1-8.6 ppm. Upon complexation with Zn(II), in the ^{1}H NMR spectrum, the presence of the indole NH proton was shifted to 12.2 ppm; the absence of the hydrazide (C=O-NH) proton shows keto-enol tautomerisation due to complexation; the azomethine proton at 8.25 ppm, aromatic protons in the range 7.1-8.6 ppm.

In the ^{1}H NMR spectrum of Ligand L4, the NH proton resonates at 11.2 ppm, the azomethine proton resonates at 8.2 ppm, and the remaining aromatic protons are in the range 7.0-8.4 ppm. Upon complexation with Zn(II), in the ^{1}H NMR spectrum of L4Zn, the NH peak shifted to 11.5 ppm, the azomethine proton shifted to 8.6 ppm, and all the aromatic protons resonated at 7.0-8.5 ppm, which reveals that no tautomerisation occurred in the Zn(II) complex, which in turn supports the FTIR data[17]. The proposed structures of all the synthesised complexes of L3 and L4 are given in **Fig. 3[(a) and (b)]** and **Fig. 4[(a) and (b)].** All the ^{1}H and ^{13}C NMR plots are given in **Fig. S11- S17.**

TGA analysis:

The thermogravimetric analysis results reveal that all the synthesised metal complexes in this work are stable up to 200°C, and a few of them are stable up to 350°C, which also supports the melting point data provided in the experimental section. The TGA was run from 27-800°C. These stable compounds can have a wide range of applications due to their thermal stability of up to 200°C, which is better than that of organic compounds.[18]

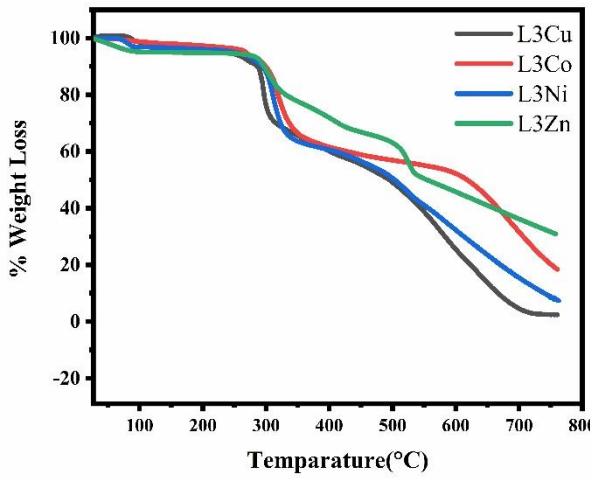

Fig. 1(a) TGA plot of Co(II), Ni(II), Zn(II) and Cu(II) Complexes of L3

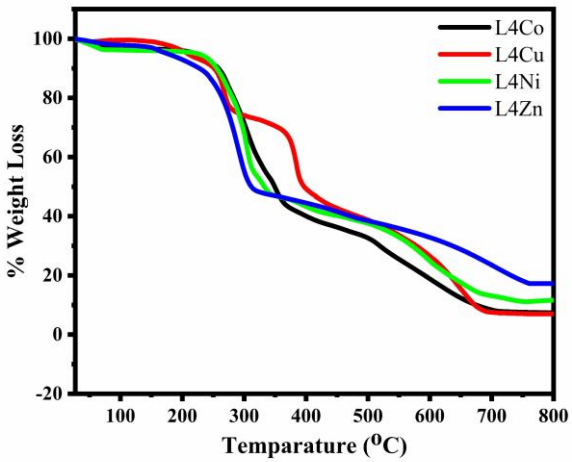

Fig. 1(b) TGA plot of Co(II), Ni(II), Zn(II) and Cu(II) Complexes of L4

UV -Visible Spectroscopy:

The ligands L3, L4 and their complexes were exposed to UV-visible spectroscopy, which reveals that the ligand L3 and its metal complexes absorb light at a wavelength of about 350–450 nm, which corresponds to the n-π* and π-π* transitions. The metal complexes exhibit a bathochromic shift; especially, the shift is much more prominent in the L3Co complex. Similarly, L4 and its complexes exhibit 2 absorption bands around 280-320nm which correspond to the n-π* and π-π* transitions. There is a reasonable increase in intensity and a bathochromic shift observed in all the complexes[19]. An overlay of these spectra is provided in **Fig.2 [(a) and (b)]** for both L3 and L4 and their respective complexes to interpret and compare the ligand and its complexes.

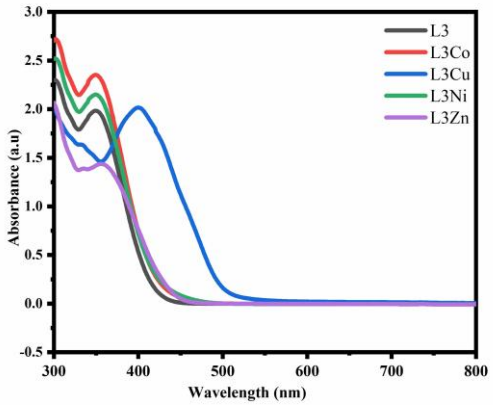

Fig. 2(a) UV-Visible plot of L3 and its Co(II), Cu(II), Ni(II), Zn(II) Complexes.

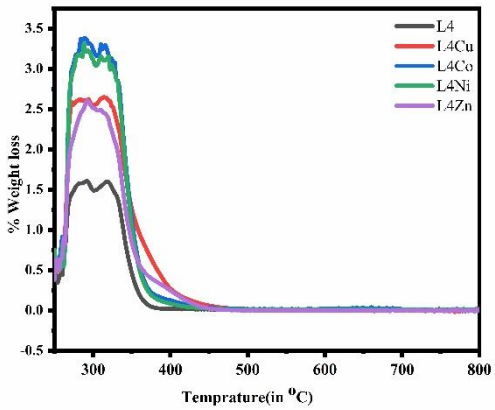

Fig. 2(b) UV-Visible plot of L4 and its Co(II), Cu(II), Ni(II), Zn(II) complexes.

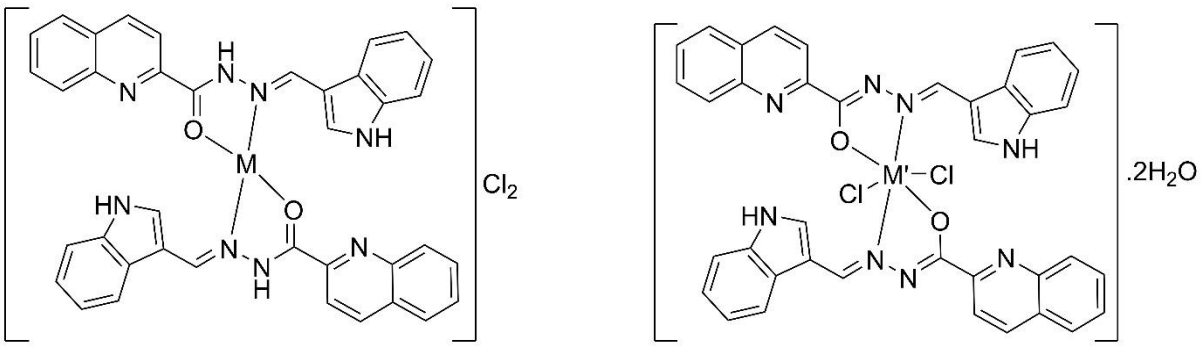

(a) **(b)**

Fig. 3 Proposed structures of metal complexes of L3, based on NMR(^{1}H and ^{13}C), Mass, TGA, and FTIR data.**(a)** Where M = Co(II) and Ni(II). **(b)** Where M′= Cu(II) and Zn(II).

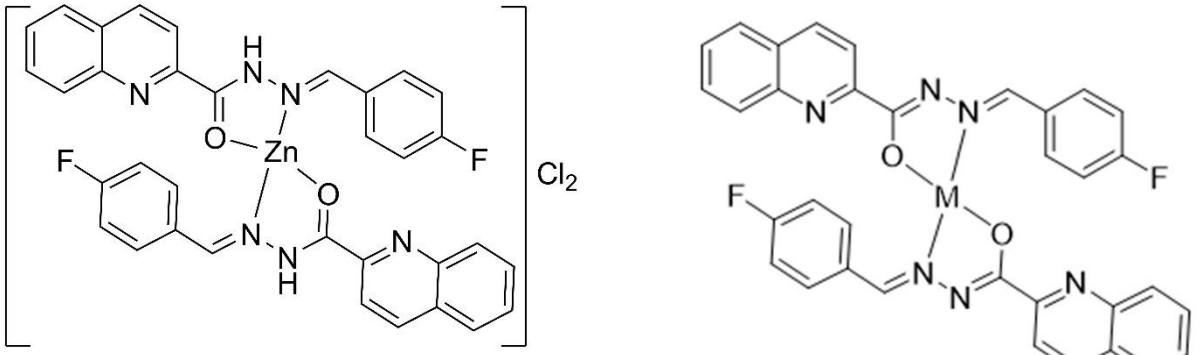

(a) **(b)**

Fig. 4. (a) Proposed structure of the Zn(II) complex of L4, based on NMR, mass spectrometry, TGA, and FTIR analyses. **(b)** Proposed general structure of the L4 complexes, where M = Co(II), Ni(II), and Cu(II).

Crystal Structure Data of L3:

The crystallisation of the ligand L3 was done using a liquid-liquid diffusion method. 10mg of the compound was dissolved in 1ml of DMF, and 2ml of ethanol was used as an antisolvent. This was kept for crystallisation in a dark place for 8 days, and yellow transparent crystals were obtained. These crystals were mounted on the Singal crystal X-ray diffractometer, analysed and the obtained results are listed in **Table 3**. The crystal has an orthorhombic crystal system. The analysis results reveal that the crystal structure formed matches the expected requirements of Ligand L3. The ORTEP diagram and the intermolecular H- bonding of ligand L3 are given in **Fig. 5 (a)** and **(b),** respectively. The bond angle data and torsion data are provided in **Tables S1** and **S2.**

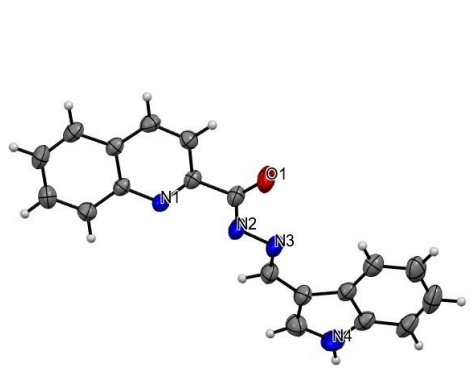

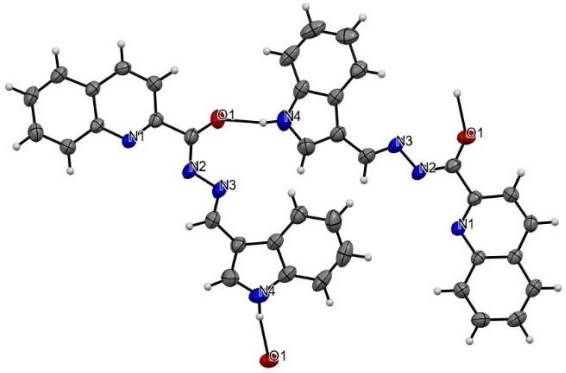

Fig. 5(a) ORTEP Diagram of L3 **Fig. 5(b)** Intermolecular Hydrogen- Bonding in L3

Table 3. Crystal structure data of L3

CCDC Deposition number	2521490
Empirical formula	C_{19} H_{14} N_4 O
Formula weight	315
Temperature (K)	283-303
Wavelength	0.71073 A^0
Colour/Appearance	Yellow crystalline
Crystal system	Orthorhombic
Space group	P b c a (61)
Packing coefficient	0.683061
Unit cell dimensions	**a**=13.1982(6) **α**=90 **b**=8.2198(4) **β**=90 **c**=28.6479(12) γ=90
Volume (A^0)	3107.91
Density	1.344
Z, Z'	**Z**: 8 **Z'**: 1
R-Factor (%)	9.09

Anti-tubercular activity

The ligand L3 and ligand L4 and their Co(II), Ni(II), Cu(II) and Zn(II) complexes were subjected to Anti-tubercular analysis. Efficacy of samples against M. tuberculosis was assessed using the microplate Alamar Blue assay (MABA)[20, 21]. The non-toxic system uses a thermally stable reagent and correlates well with proportional and BACTEC radiometric methods. The 96-well plate was incubated at 37ºC for five days, followed by a 24-hour incubation with a mixture of Alamar Blue reagent and 10 to 80[22]. The MIC was defined as the lowest concentration of the medicine. The aforementioned figures indicate that our compounds demonstrate anti-tubercular activity, albeit at higher concentrations than the typical medications that are FDA-approved[18, 23, 24]. However, a few samples, including ligands and complexes, have shown this property at a concentration of 50 µg/mL, which medical advisors deem acceptable. Also, L3Ni and L4Ni have shown activity at lower concentrations, which makes the point that Ni(II) has potent anti-tubercular activity when compared to the other 3 metals Co(II), Cu(II) and Zn(II). The Activity results are given in **Fig. 6 and 7.** The graphical representation is given in **Fig. 8**.

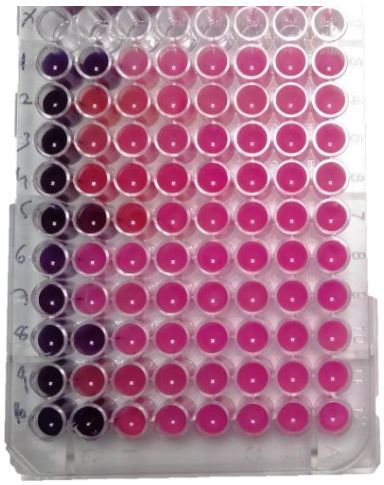

Fig. 6 Antibacterial activity of samples (L3, L4 and their complexes) at varying concentrations (100 to 0.8 µg/mL)

Fig. 7 Antibacterial sctivity of standard antibacterial drugs and their critical Concentrations

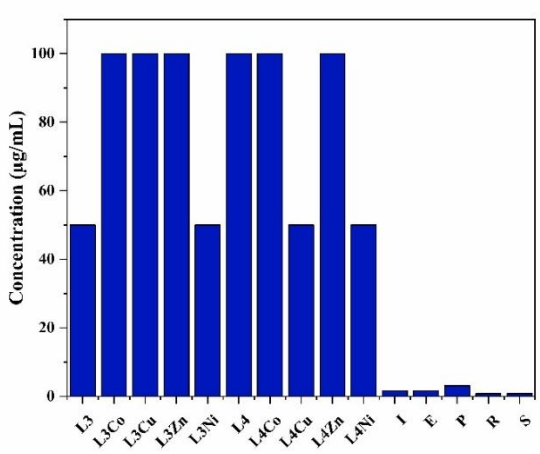

Fig. 8 Graphical representation of Antitubercular activity of L3, L4 and their complexes with standard drugs

Anti-cancer activity of ligands and their copper complexes.

Cancer is a leading cause of death worldwide, with breast cancer—especially the aggressive triple-negative breast cancer (TNBC) subtype—presenting major therapeutic challenges due to drug resistance, poor bioavailability, and severe side effects from conventional treatments like platinum-based chemotherapeutics[25, 26]. TNBC lacks expression of estrogen receptor, progesterone receptor, and HER2, leading to high metastasis rates and poor prognosis, with no effective targeted therapies available for advanced cases[27]. Copper-based quinoline organometallic complexes have emerged as promising alternatives, leveraging copper's role in reactive oxygen species generation and apoptosis induction for selective cancer cell cytotoxicity[28]. This study assessed the anticancer activity of quinoline-derived samples L3, L3Cu, L4, and L4Cu against TNBC MDA-MB-231 cells using MTT assay, with cisplatin as the positive control and untreated cells as negative control[29]. As there have been previous results that copper complexes exhibit better anticancer activity when compared to other inner transition metal complexes[29–31].

The compounds demonstrated a dose-dependent reduction in cell viability across 10–50 µg/mL concentrations. Specifically, at 10 µg/mL, viability percentages were 62.75±0.0049% for L3, 58.66±0.0063% for L3Cu, 69.57±0.0045% for L4, and 60.84±0.0091% for L4Cu. Increasing to 50 µg/mL resulted in significantly lower viabilities: 12.27±0.0035% (L3), 12.68±0.0042% (L3Cu), 16.09±0.0025% (L4), and 13.09±0.0063% (L4Cu), closely comparable to cisplatin's 9.004±0.0212% at the same dose.

IC50 values underscored the potency of these compounds: L3Cu at 15.55 µg/mL, L4Cu at 18.13 µg/mL, L3 at 18.45 µg/mL, and L4 at 24.85 µg/mL, indicating L3Cu, L3, and L4Cu as particularly effective with lower IC_{50} values relative to the standard. Microscopic examination of treated cells revealed distinct morphological alterations, including cell shrinkage, elongation, and formation of apoptotic bodies with dead cells, markedly differing from the morphology of untreated controls and aligning with cisplatin's effects**.** The percentage cell viability data is given in **Table 4**; IC_{50} values of ligands and their copper(II) complexes are given in **Table 5** and inhibition images are given in **Fig. 9(a-f)**. The percentage cell viability graphical representation is given in **Fig. S18 - S21**.

Table 4. Percentage of Cell viability of the triple-negative breast cancer MDAMB-231 cell line treated with test sample.

Sl.No	Concentration (µg/mL)	L3	L3Cu	L4	L4Cu
1	10	62.75±0.0049	58.66±0.0063	69.57±0.0045	60.84±0.0091
2	20	46.52±0.0056	43.79±0.0028	55.25±0.0040	46.38±0.0035
3	30	33.28±0.0035	30.96±0.0042	43.65±0.0035	34.37±0.0063
4	40	23.73±0.0021	21.00±0.0035	31.92±0.0025	27.28±0.0049
5	50	12.27±0.0035	12.68±0.0042	16.09±0.0025	60.84±0.0091

Standard drug Cisplatin at 15µg/mL shows cell viability 12.94±0.0035

Table 5. IC_{50} of test samples for triple negative breast cancer MDAMB-231

Sample name	MDAMB-231 cell line IC_{50} (in µg/ml) 24hr
L3	18.45
L3Cu	**15.55**
L4	24.85
L4Cu	18.13

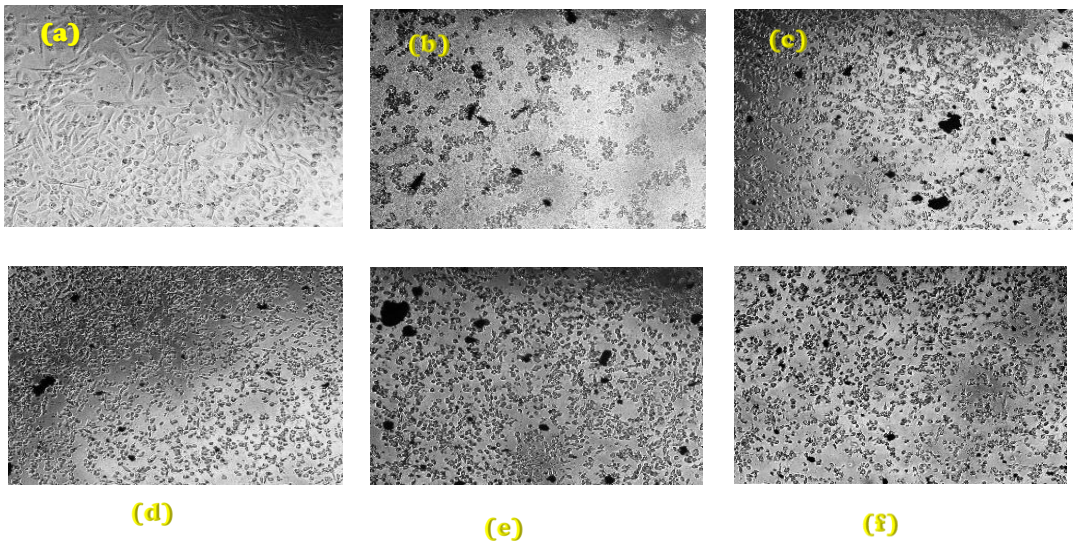

Fig. 9 Anticancer activity of test samples at higher concentrations: where, (a) Untreated, (b)Cisplatin, (c) L3, (d) L3Cu, (e) L4, (f) L4Cu

Conclusion:

The ligands L3 and L4 were synthesized and subjected to various spectroscopic techniques to verify that the synthesized compounds matched the suggested structures. They were complexed with Co(II), Ni(II), Cu(II), and Zn(II) complexes, all of which mostly have ML_2 type geometry with some substituents on the side. A few complexes underwent tautomerization after complexation, which was verified by FTIR and ^{1}H NMR data of Zn(II) complexes. Studies on anti-tubercular activity show that Ni(II) complexes are more sensitive even at lower concentrations. Additionally, both ligands and their corresponding Cu(II) complexes were tested for anti-cancer efficacy against the MDA-MB-231 cell line; the findings indicate IC_{50} values < 25µg/ml. The difference between the ligands' IC_{50} values and their copper complexes is visible, suggesting that complexation with copper lowers the IC_{50} values.

Highlights

- Synthesis and characterization of hydrazone-based ligands and its transition metal complexes.
- The crystal structure of the L3 ligand is confirmed by single-crystal XRD technique.
- All the test compounds show anti-tubercular activity, but L3, L3Ni, L4Cu, and L4Ni exhibit activity at 100µg/ml concentrations.
- The ligands and their copper(II) complexes show anti-breast cancer activity and obtain good IC_{50} values below 25.

Acknowledgements:

The author is grateful to Karnatak University, Dharwad, for awarding the University Research Studentship and thankful to USIC, K.U. Dharwad for providing single-crystal X-ray diffraction and other instrumentation facilities. Also, to the Central University of Hyderabad and Central University of Karnataka, Kalaburgi, for providing necessary help.

Funding:

University Research Studentship, Karnatak University, Dharwad.

Conflict of interest:

The authors do not have any conflict of interest.

Declaration of generative AI in scientific writing

Generative AI has been used only in refining the written manuscript by using only editing and polishing the manuscript. It was not used in scientific processes or any discrete writing and drawing conclusions.

Authors' contributions:

Laxmi A Jagatap: Conceptualization, Data curation, Formal analysis, Methodology, Writing – original draft, Writing – review & editing; Shivaraj S Dolli: Data curation, Formal analysis; Ramesh Vadavi: Investigation, Methodology, Validation, Visualization; Arun K Shettar and Joy H Hoskeri Methodology, Validation, writing, Resourses; Oruganti Anjaneyulu: Data curation, Formal analysis, Investigation, Resources, Supervision, Validation; Kalagauda Gudasi: Conceptualization, Data curation, Formal analysis, Investigation, Resources, Software, Supervision, Validation.

References:

[1]. World Health Organization. (2025). *Global Tuberculosis Report 2025.* World Health Organization, Geneva.

[2]. World Health Organization. (2026). *Global Status Report on Cancer 2026: The Future We Choose Together.* World Health Organization, Geneva.

[3]. Aragón-Muriel, A., Reyes-Márquez, V., Cañavera-Buelvas, F., Parra-Unda, J.R., Cuenú-Cabezas, F., Polo-Cerón, D., Colorado-Peralta, R., Suárez-Moreno, G.V., Aguilar-Castillo, B.A., Morales-Morales, D. (2022). Pincer Complexes Derived from Tridentate Schiff Bases for Their Use as Antimicrobial Metallopharmaceuticals. *Inorganics* 10(9): 134. DOI: 10.3390/inorganics10090134.

[4]. Camellia, F.K., Ashrafuzzaman, Md., Islam, Md.N., Banu, L.A., Kudrat-E-Zahan, Md. (2022). Synthesis, Characterization, Antibacterial and Antioxidant Studies of Isoniazid-Based Schiff Base Ligands and Their Metal Complexes. *Asian Journal of Applied Chemistry Research* 11(3): 8–23.

[5]. Aroua, L.M., Alhag, S.K., Al-Shuraym, L.A., Messaoudi, S., Mahyoub, J.A., Alfaifi, M.Y., Al-Otaibi, W.M. (2023). Synthesis and Characterization of Different Complexes Derived from Schiff Base and Evaluation as a Potential Anticancer, Antimicrobial, and Insecticide Agent. *Saudi Journal of Biological Sciences* 30(3): 103598.

[6]. Mohan, A.P., Viju Kumar, V.G., Meenukutty, M.S., Vidya, V.G. (2024). Novel Schiff Base as Potent Antimalarial: Synthesis, Single Crystal X-ray Structure, Spectroscopic Analysis, Theoretical Investigation and Molecular Docking Studies. *Results in Chemistry* 11: 101852. DOI: 10.1016/j.rechem.2024.101852.

[7]. Bingul, M., Tan, O., Gardner, C.R., Sutton, S.K., Arndt, G.M., Marshall, G.M., Cheung, B.B., Kumar, N., Black, D.S.C. (2016). Synthesis, Characterization and Anti-Cancer Activity of Hydrazide Derivatives Incorporating a Quinoline Moiety. *Molecules* 21(7): 916. DOI: 10.3390/molecules21070916.

[8]. Tafere, D.A., Gebrezgiabher, M., Elemo, F., Sani, T., Atisme, T.B., Ashebr, T.G., Ahmed, I.N. (2025). Hydrazones, Hydrazones-Based Coinage Metal Complexes, and Their Biological Applications. *RSC Advances* 15: 6191–6207. DOI: 10.1039/D4RA07794F.

[9]. Kumar, B., Devi, J., Dubey, A., Tufail, A., Taxak, B. (2023). Investigation of Antituberculosis, Antimicrobial, Anti-Inflammatory Efficacies of Newly Synthesized Transition Metal(II) Complexes of Hydrazone Ligands: Structural Elucidation and Theoretical Studies. *Scientific Reports* 13: 15906. DOI: 10.1038/s41598-023-42180-4.

[10]. Božić, A., Marinković, A., Bjelogrlić, S., Todorović, T.R., Cvijetić, I.N., Novaković, I., Muller, C.D., Filipović, N.R. (2016). Quinoline Based Mono- and Bis-(Thio)Carbohydrazones: Synthesis, Anticancer Activity in 2D and 3D Cancer and Cancer Stem Cell Models. *RSC Advances* 6: 104763–104781. DOI: 10.1039/C6RA23940D.

[11]. [11] Shruthi, T.G., Subramanian, S., Eswaran, S. (2020). Design, Synthesis and Study of Antibacterial and Antitubercular Activity of Quinoline Hydrazone Hybrids. *Heterocyclic Communications* 26(1): 137–147. DOI: 10.1515/hc-2020-0109.

[12]. [12] Kumari, P.T., TCM, Y., Krishnamurthy, C., Shekharagouda, P. (2026). Novel Fluorescent Quinoline-Based Hydrazone Metal Complexes: Synthesis, Photophysical Applications in Latent Fingerprint Detection, Anti-Counterfeiting, and Antitubercular Activity. *Journal of Molecular Structure* 1356: 145146. DOI: 10.1016/j.molstruc.2025.145146.

[13]. Jagatap, L.A., Vadavi, R., Dolli, S.S., Ilkal, V., Ankala Basappa, V., Bhat, S.S., Anjaneyulu, O., Gudasi, K. (2026). Coordination Behavior and Biological Potential of Co(II), Cu(II), Ni(II) and Zn(II) Complexes of 2-Substituted Quinoline Hydrazone Ligands. *Journal of Coordination Chemistry* (published online 17 July 2026): 1–16.

[14]. Nguyen, Q.T., Pham Thi, P.N., Do Bui, Q., Nguyen, V.T. (2023). Synthesis, Spectral Characterization, and Biological Activities of Some Metal Complexes Bearing an Unsymmetrical Salen-Type Ligand, (Z)-1-(((2-((E)-(2-Hydroxy-6-methoxybenzylidene)amino)phenyl)amino)methylene)naphthalen-2(1H)-one. *Heteroatom Chemistry* 2023: 4563958. DOI: 10.1155/2023/4563958.

[15]. McIndoe, J.S., Vikse, K.L. (2019). Assigning the ESI Mass Spectra of Organometallic and Coordination Compounds. *Journal of Mass Spectrometry* 54(5): 466–479. DOI: 10.1002/jms.4359.

[16]. Kendur, U., Chimmalagi, G.H., Patil, S.M., Gudasi, K.B., Frampton, C.S. (2018). Synthesis, Structural Characterization and Biological Evaluation of Mononuclear Transition Metal Complexes of Zwitterionic Dehydroacetic Acid N-Aroylhydrazone Ligand. *Applied Organometallic Chemistry* 32(4): e4278. DOI: 10.1002/aoc.4278.

[17]. Gudasi, K.B., Patil, S.A., Vadavi, R.S., Shenoy, R.V., Patil, M.S. (2006). Synthesis and Spectral Studies of Cu(II), Ni(II), Co(II), Mn(II), Zn(II) and Cd(II) Complexes of a New Macrocyclic Ligand N,N′-Bis(2-Benzothiazolyl)-2,6-Pyridinedicarboxamide. *Journal of the Serbian Chemical Society* 71(5): 529–542.

[18]. Bartzatt, R. (2016). Potency and Properties of Hydrazide Compounds That Inhibit the Growth of *Mycobacterium tuberculosis*. *Journal of Advances in Medical and Pharmaceutical Sciences* 11(1): 1–9.

[19]. Mandewale, M.C., Thorat, B., Shelke, D., Yamgar, R. (2015). Synthesis and Biological Evaluation of New Hydrazone Derivatives of Quinoline and Their Cu(II) and Zn(II) Complexes against *Mycobacterium tuberculosis*. *Bioinorganic Chemistry and Applications* 2015: 153015. DOI: 10.1155/2015/153015.

[20]. Collins, L.A., Franzblau, S.G. (1997). Microplate Alamar Blue Assay versus BACTEC 460 System for High-Throughput Screening of Compounds against *Mycobacterium tuberculosis* and *Mycobacterium avium*. *Antimicrobial Agents and Chemotherapy* 41(5): 1004–1009. DOI: 10.1128/AAC.41.5.1004.

[21]. Leonard, B., Coronel, J., Siedner, M., Grandjean, L., Caviedes, L., Navarro, P., Gilman, R.H., Moore, D.A.J. (2008). Inter- and Intra-Assay Reproducibility of Microplate Alamar Blue Assay Results for Isoniazid, Rifampicin, Ethambutol, Streptomycin, Ciprofloxacin, and Capreomycin Drug Susceptibility Testing of *Mycobacterium tuberculosis*. *Journal of Clinical Microbiology* 46(10): 3526–3529. DOI: 10.1128/JCM.02083-07.

[22]. Franzblau, S.G., Witzig, R.S., McLaughlin, J.C., Torres, P., Madico, G., Hernandez, A., Degnan, M.T., Cook, M.B., Quenzer, V.K., Ferguson, R.M., Gilman, R.H. (1998). Rapid, Low-Technology MIC Determination with Clinical *Mycobacterium tuberculosis* Isolates by Using the Microplate Alamar Blue Assay. *Journal of Clinical Microbiology* 36(2): 362–366. DOI: 10.1128/JCM.36.2.362-366.1998.

[23]. Werngren, J., Sturegård, E., Juréen, P., Ängeby, K., Hoffner, S., Schön, T. (2012). Reevaluation of the Critical Concentration for Drug Susceptibility Testing of *Mycobacterium tuberculosis* against Pyrazinamide Using Wild-Type MIC Distributions and *pncA* Gene Sequencing. *Antimicrobial Agents and Chemotherapy* 56(3): 1253–1257. DOI: 10.1128/AAC.05894-11.

[24]. Gumbo, T. (2010). New Susceptibility Breakpoints for First-Line Antituberculosis Drugs Based on Antimicrobial Pharmacokinetic/Pharmacodynamic Science and Population Pharmacokinetic Variability. *Antimicrobial Agents and Chemotherapy* 54(4): 1484–1491. DOI: 10.1128/AAC.01474-09.

[25]. Błaszczak, E., Miziak, P., Odrzywolski, A., Baran, M., Gumbarewicz, E., Stepulak, A. (2025). Triple-Negative Breast Cancer Progression and Drug Resistance in the Context of Epithelial–Mesenchymal Transition. *Cancers* 17(2): 228. DOI: 10.3390/cancers17020228.

[26]. Jain, A., Barge, A., Parris, C.N. (2025). Combination Strategies with PARP Inhibitors in BRCA-Mutated Triple-Negative Breast Cancer: Overcoming Resistance Mechanisms. *Oncogene* 44: 193–207. DOI: 10.1038/s41388-024-03227-6.

[27]. Jie, H., Ma, W., Huang, C. (2025). Diagnosis, Prognosis, and Treatment of Triple-Negative Breast Cancer: A Review. *Breast Cancer: Targets and Therapy* 17: 265–274. DOI: 10.2147/BCTT.S516542.
[28]. Azimi, S.G., Shakour, N., Bagherzade, G., Saberi, M.R., Azimi, H., Moosavi F., M. (2025). A Comprehensive Review of the Biological Activities of Medicinal Metal Complexes Synthesized from Quinoline Scaffolds. *Bioinorganic Chemistry and Applications* 2025: 3133615. DOI: 10.1155/bca/3133615.
[29]. Hangan, A.C., Oprean, L.S., Procopciuc, L.M., Dican, L., Gog-Bogdan, S., Lucaciu, R.L. (2026). Copper Complexes: Main Mechanisms as Anticancer Agents. *Molecules* 31(5): 874. DOI: 10.3390/molecules31050874.
[30]. Huang, K.B., Wang, F.Y., Lu, Y., Yang, L.M., Long, N., Wang, S.S., Xie, Z., Levine, M., Zou, T., Sessler, J.L., Liang, H. (2024). Cu(II) Complex That Synergistically Potentiates Cytotoxicity and an Antitumor Immune Response by Targeting Cellular Redox Homeostasis. *Proceedings of the National Academy of Sciences of the United States of America* 121(24): e2404668121. DOI: 10.1073/pnas.2404668121.
[31]. Ribeiro, N., Bulut, I., Sergi, B., Pósa, V., Spengler, G., Sciortino, G., André, V., Ferreira, L.P., Biver, T., Ugone, V., Garribba, E., Costa-Pessoa, J., Enyedy, É.A., Acilan, C., Correia, I. (2023). Promising Anticancer Agents Based on 8-Hydroxyquinoline Hydrazone Copper(II) Complexes. *Frontiers in Chemistry* 11: 1106349. DOI: 10.3389/fchem.2023.1106349.

Supplementary Information

FTIR Data:

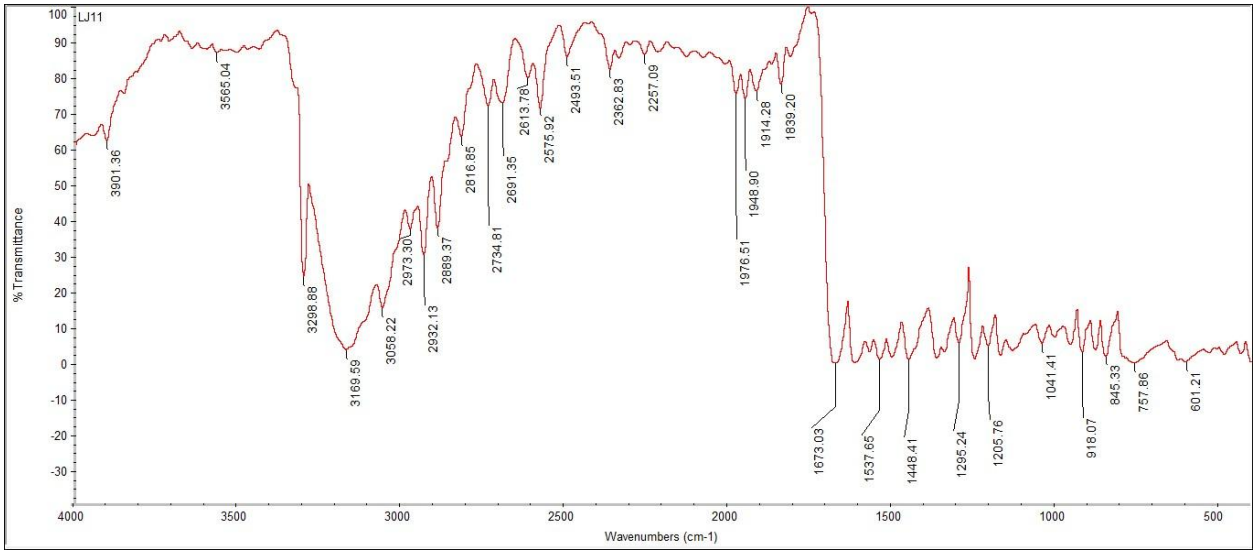

Fig. S1 *FTIR data of ligand L3*

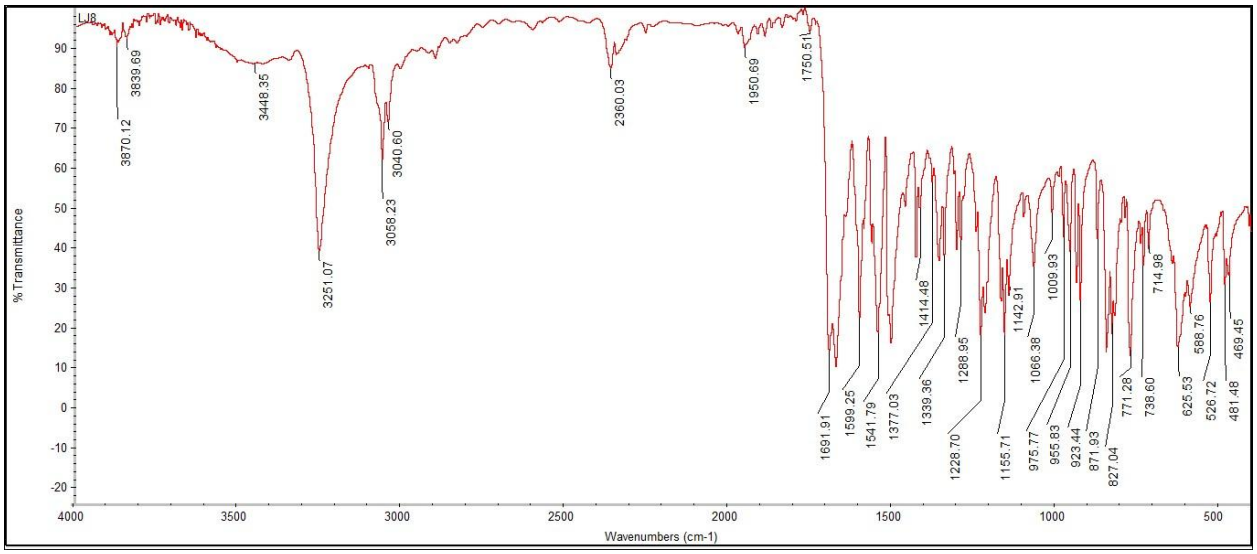

Fig. S2 *FTIR data of ligand L4*

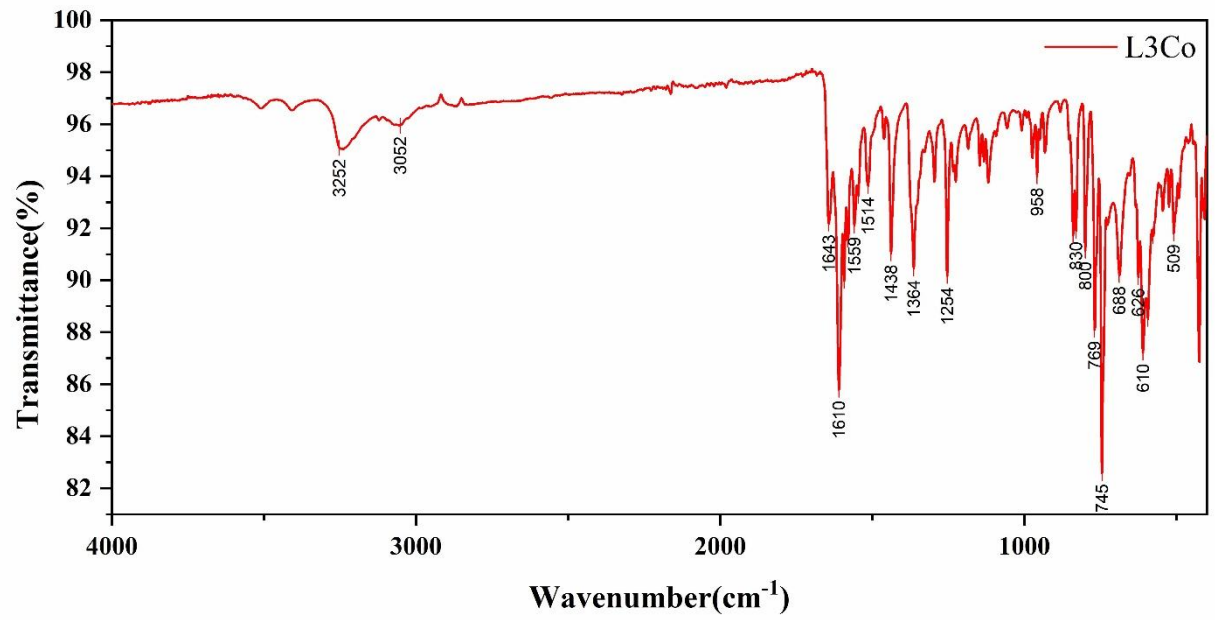

Fig. S3 *FTIR data of L3Co*

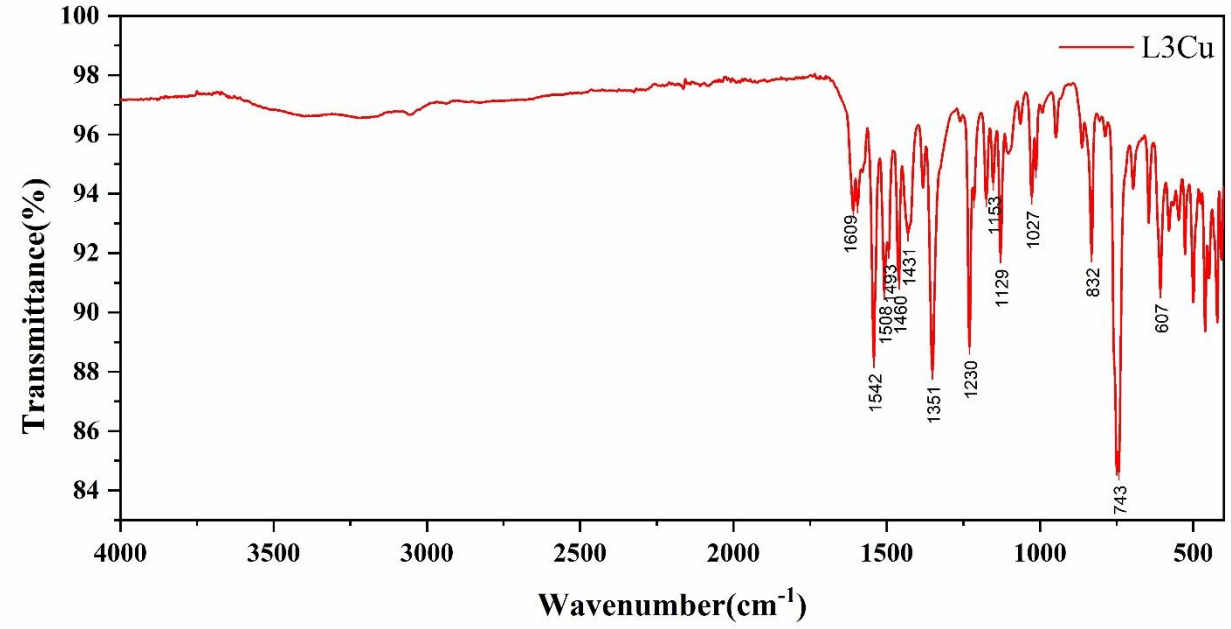

Fig. S4 *FTIR data of L3Cu*

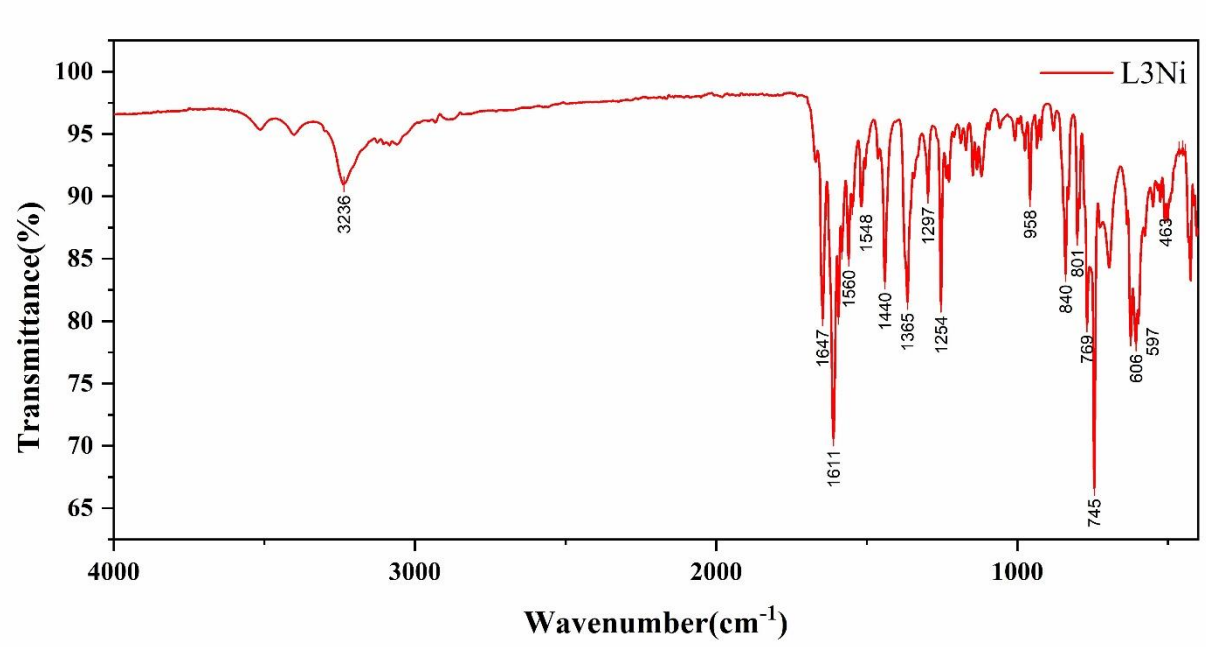

Fig. S5 *FTIR data of L3Ni*

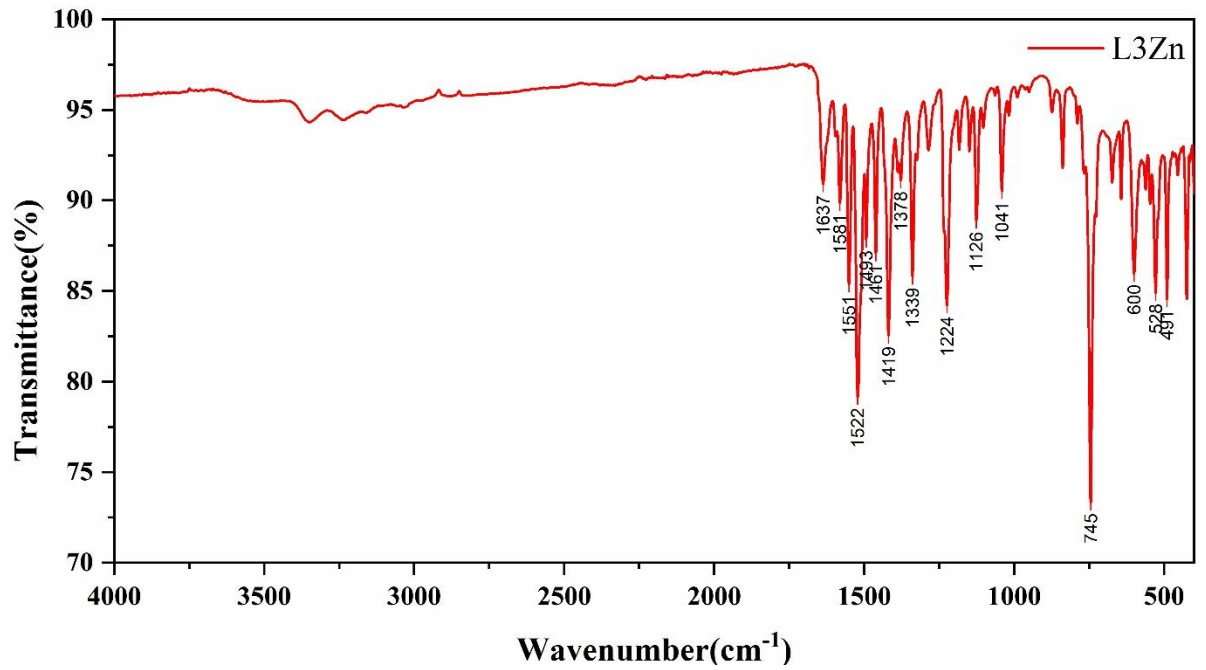

Fig. S6 *FTIR data of L3Zn*

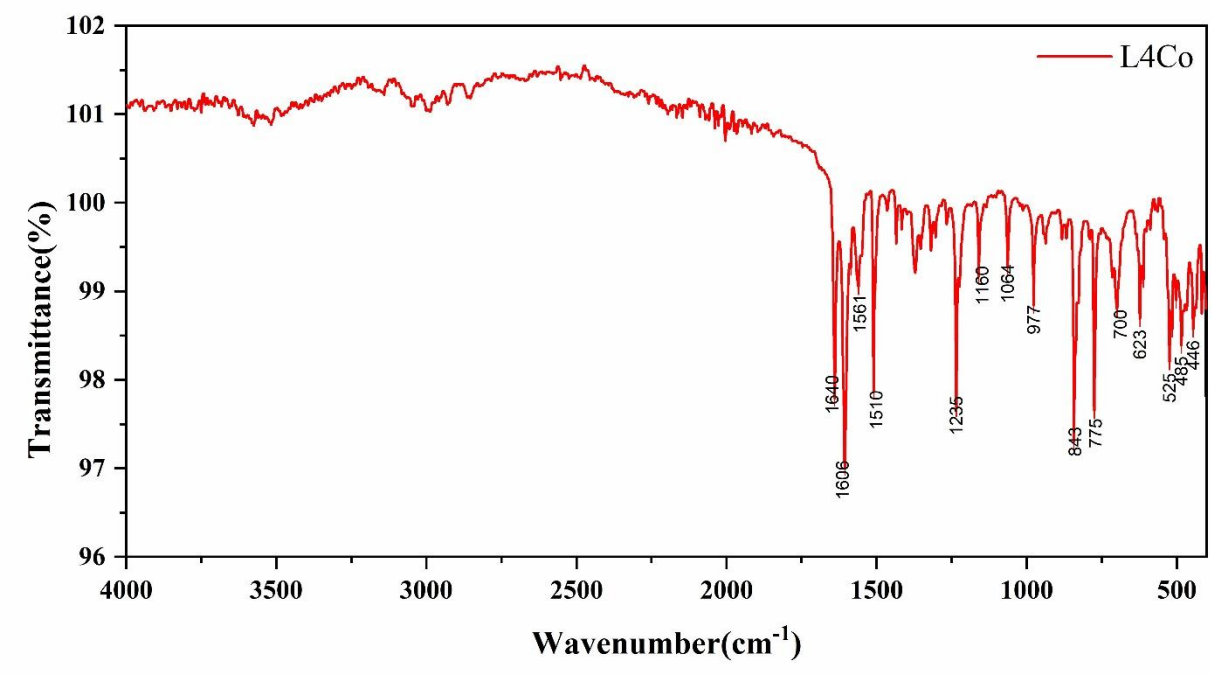

Fig. S7 *FTIR data of L4Co*

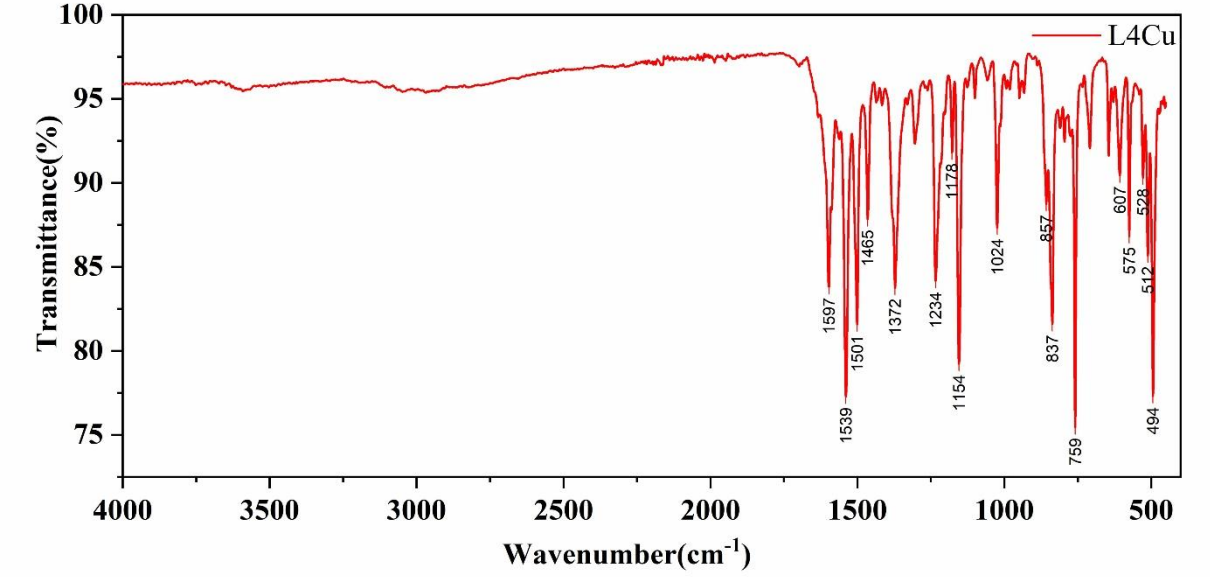

Fig. S8 *FTIR data of L4Cu*

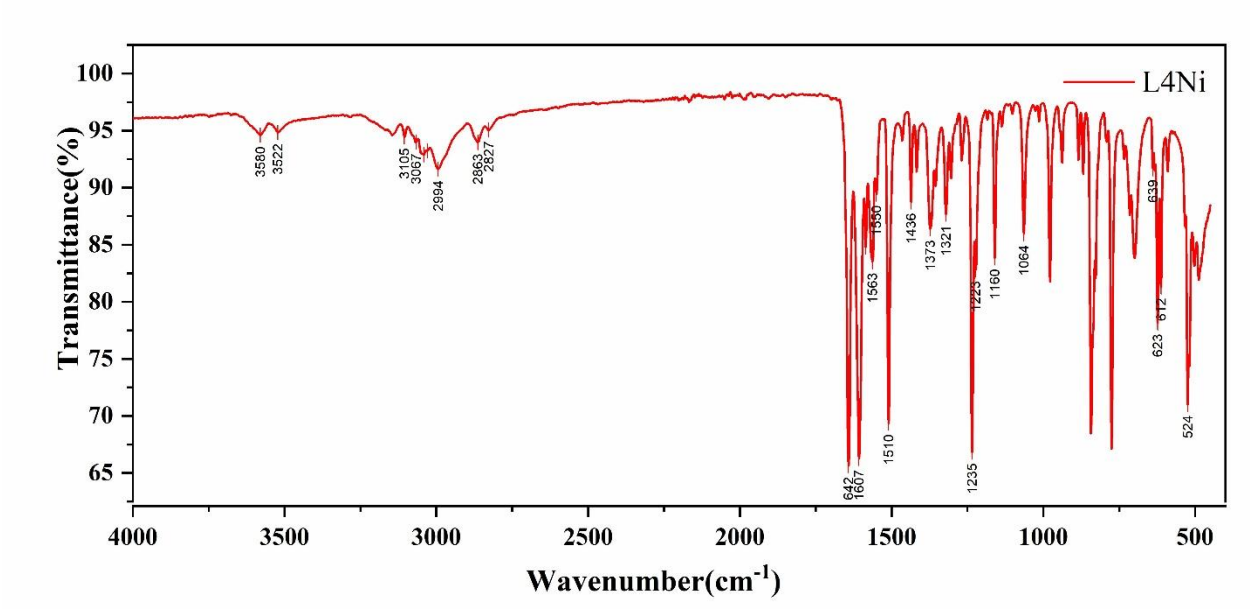

Fig. S9 *FTIR data of L4Ni*

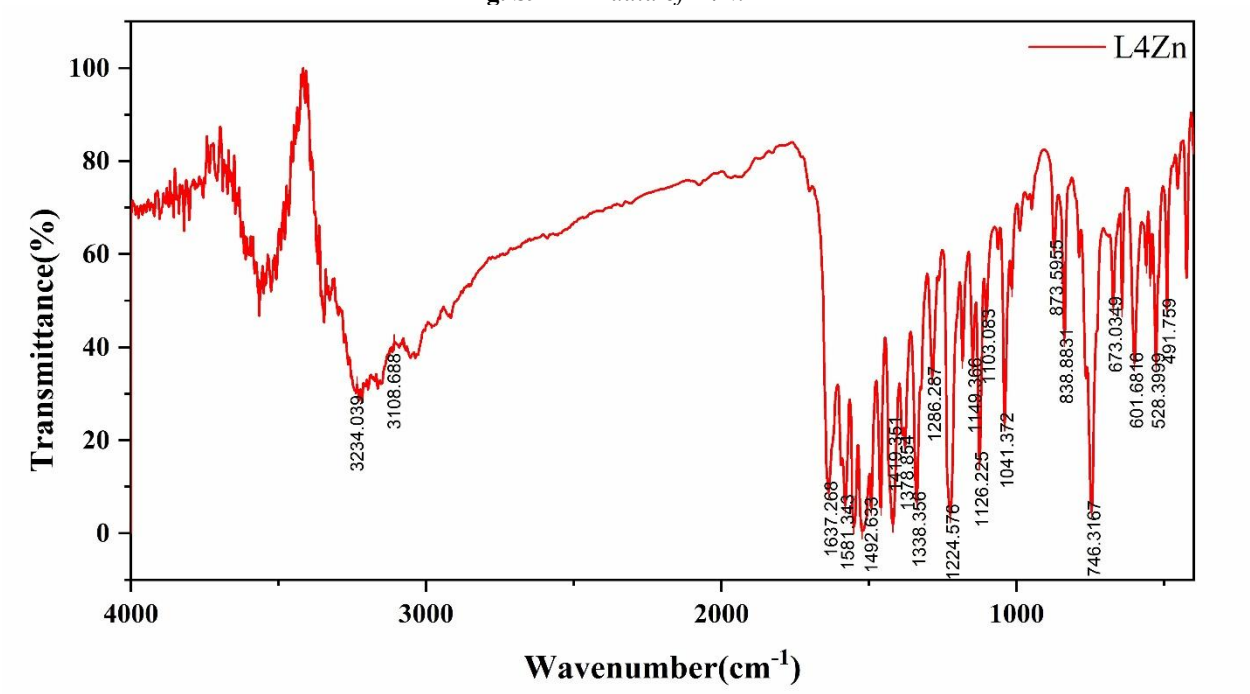

Fig. S10 *FTIR data of L4Zn*

NMR Data

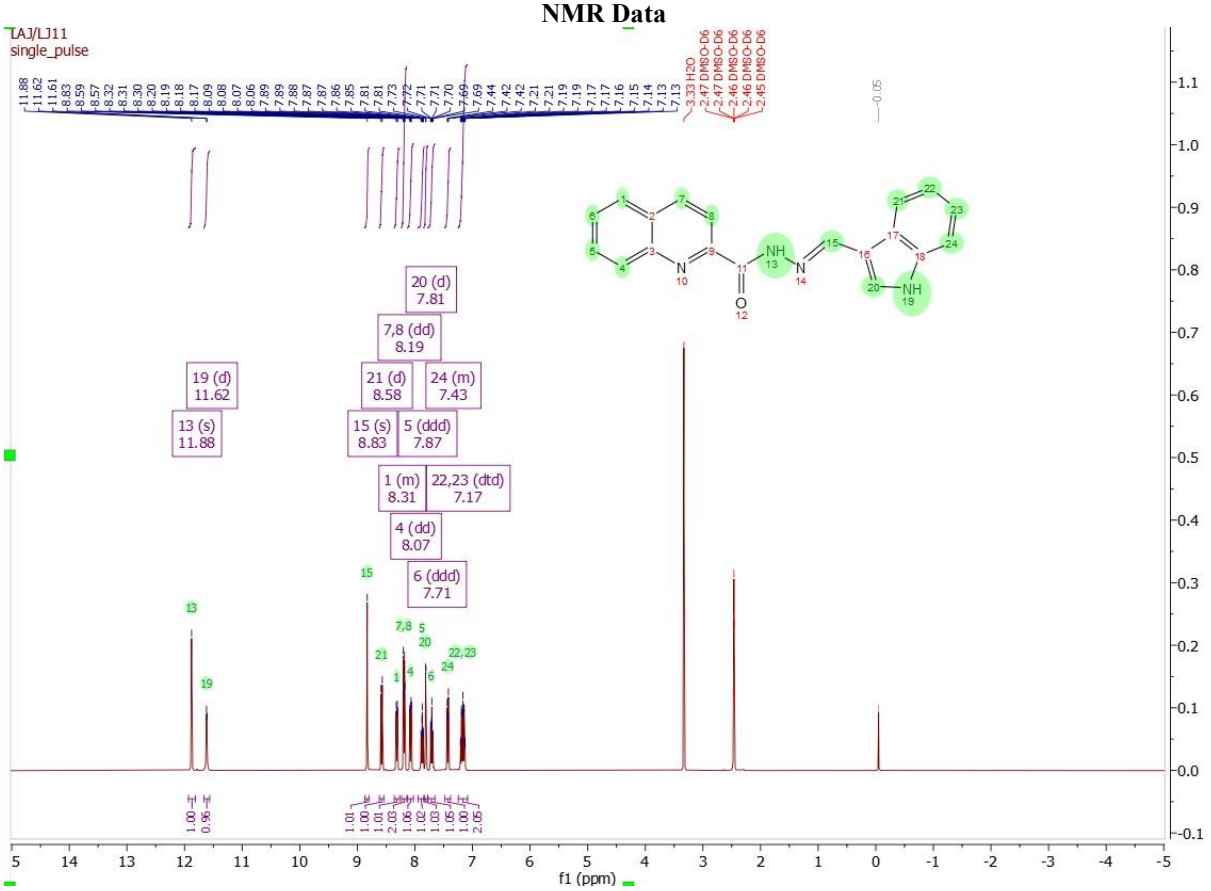

Fig. S11 ^{1}H NMR Spectrum of L3

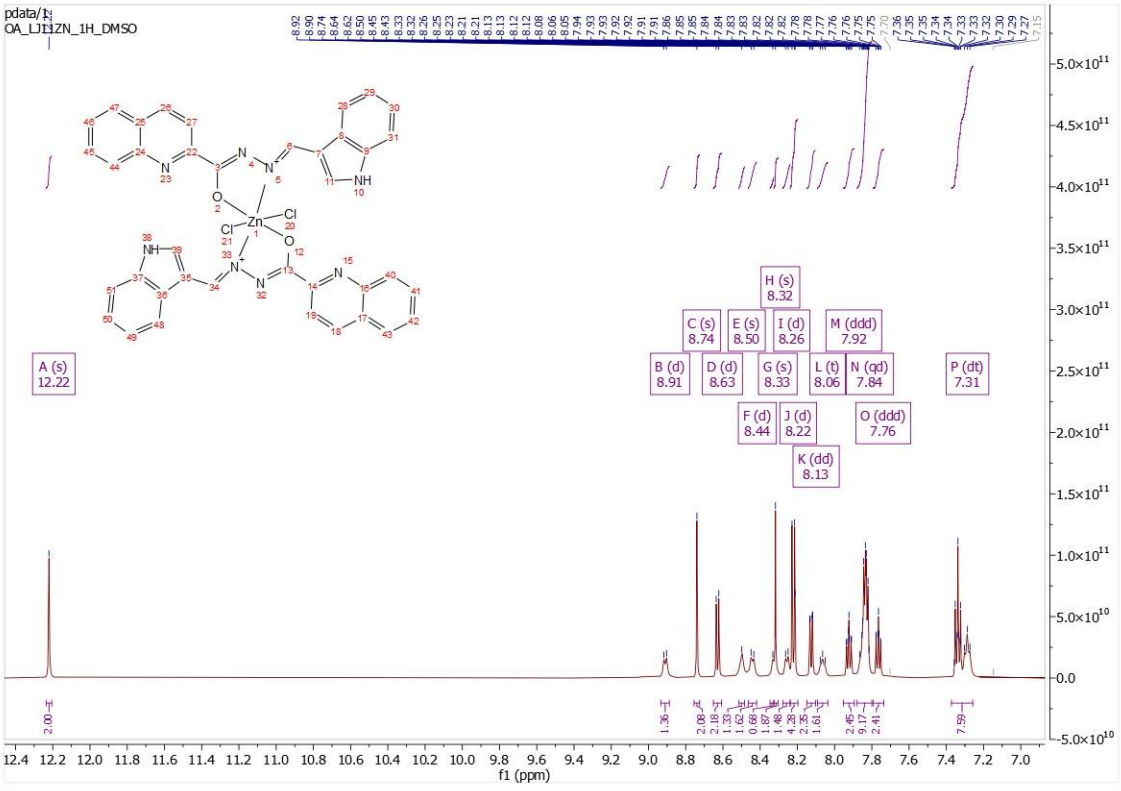

Fig. S12 ^{13}C NMR Spectrum of L3

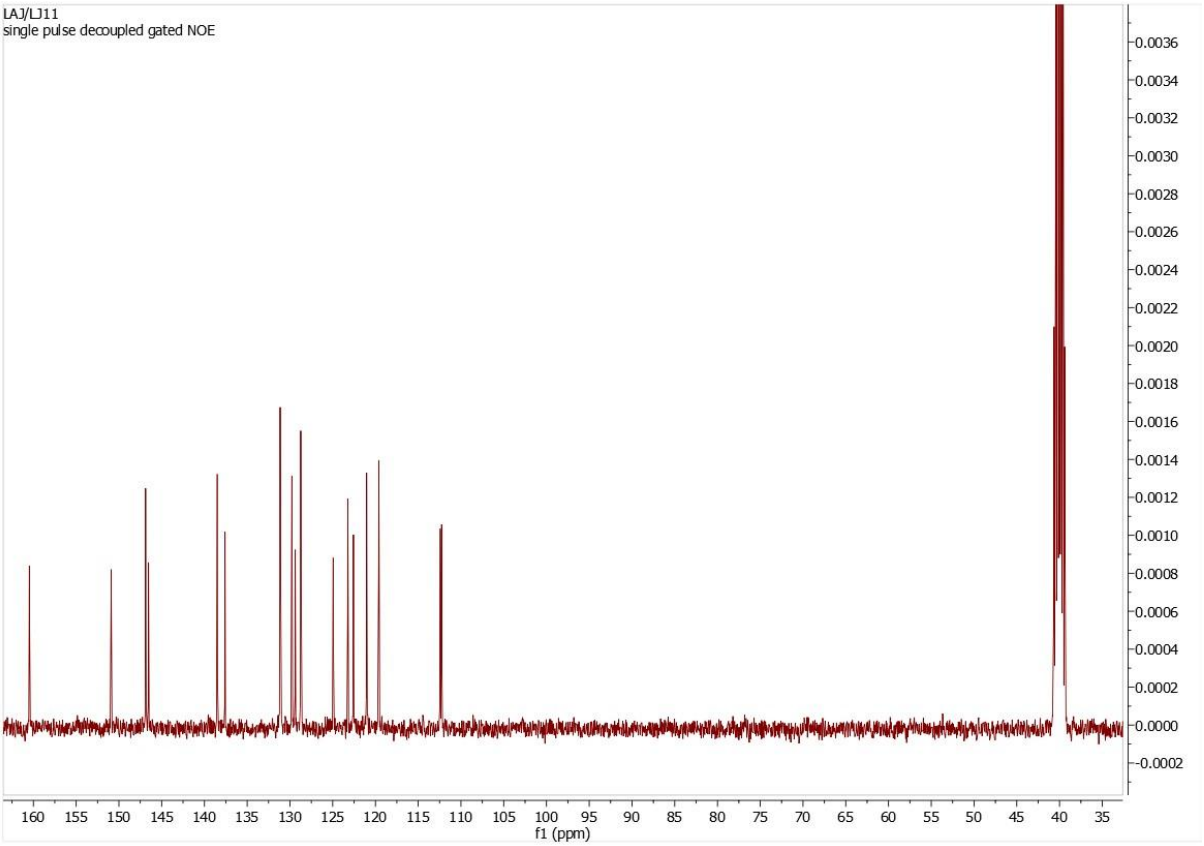

Fig. S13 ^{1}H NMR Spectrum of L3Zn

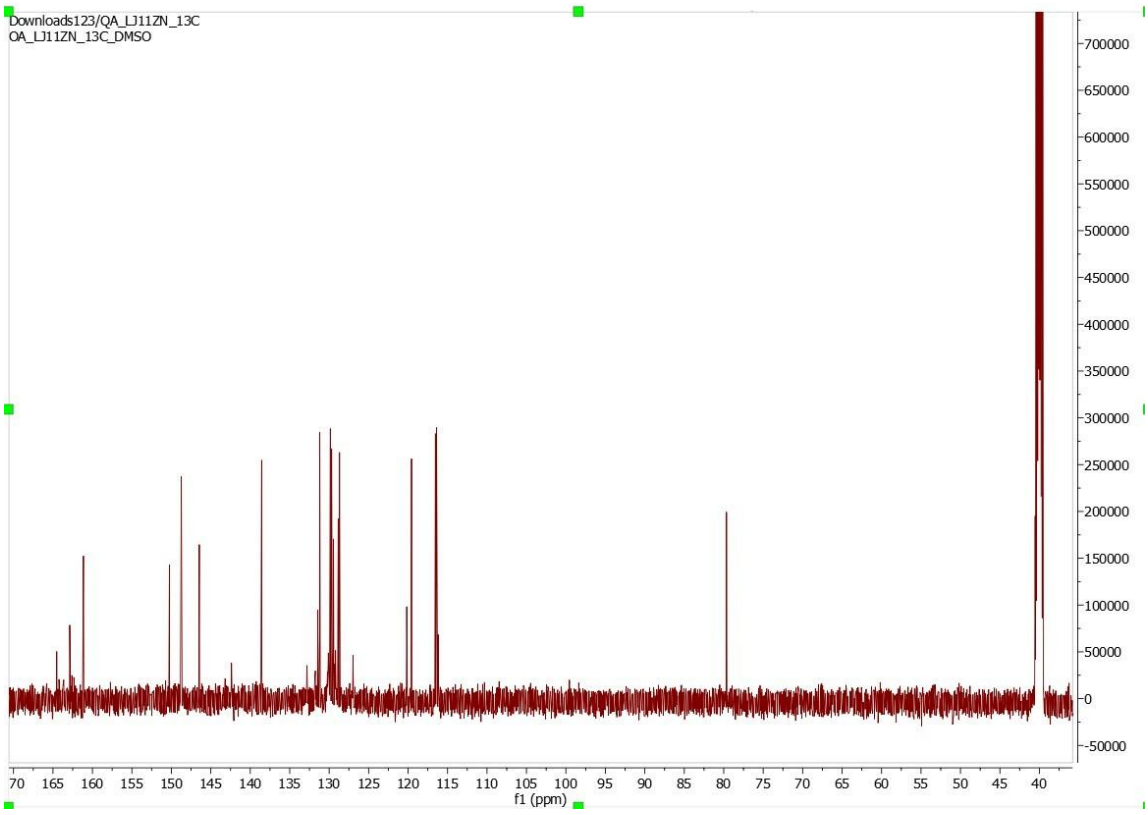

Fig. S14 ^{13}C NMR Spectrum of L3Zn

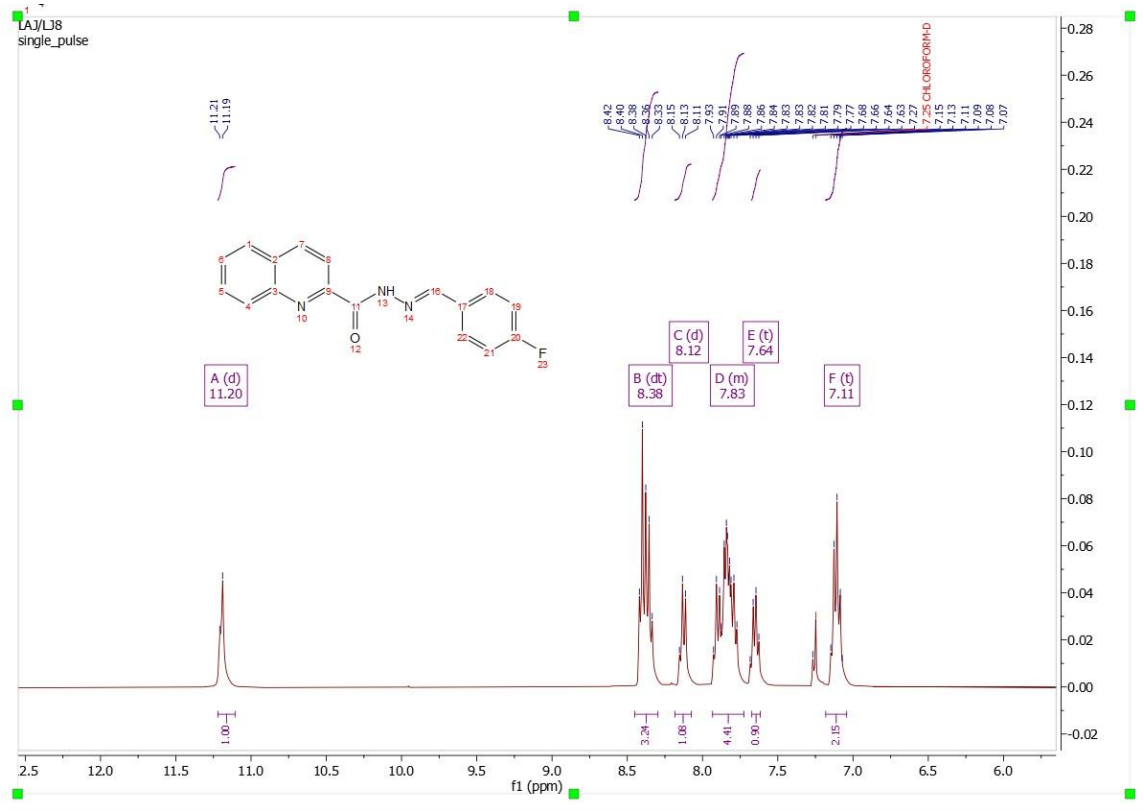

Fig. S15 ^{1}H NMR Spectrum of L4

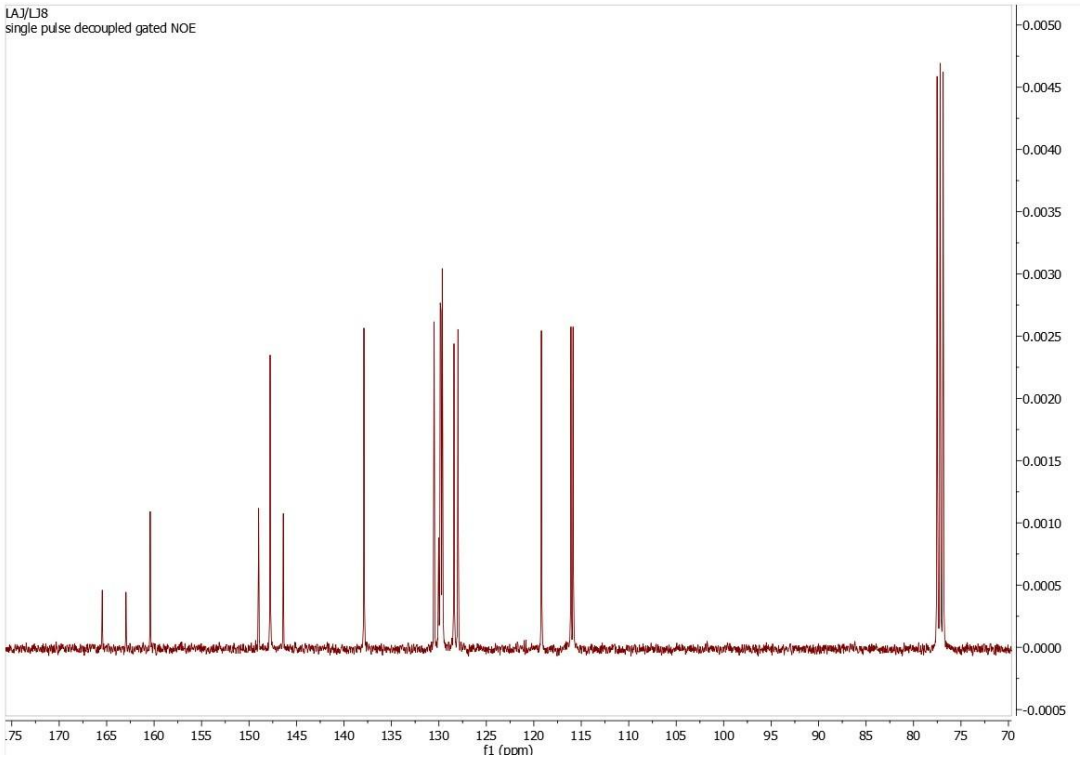

Fig. S16 ^{13}C NMR Spectrum of L4

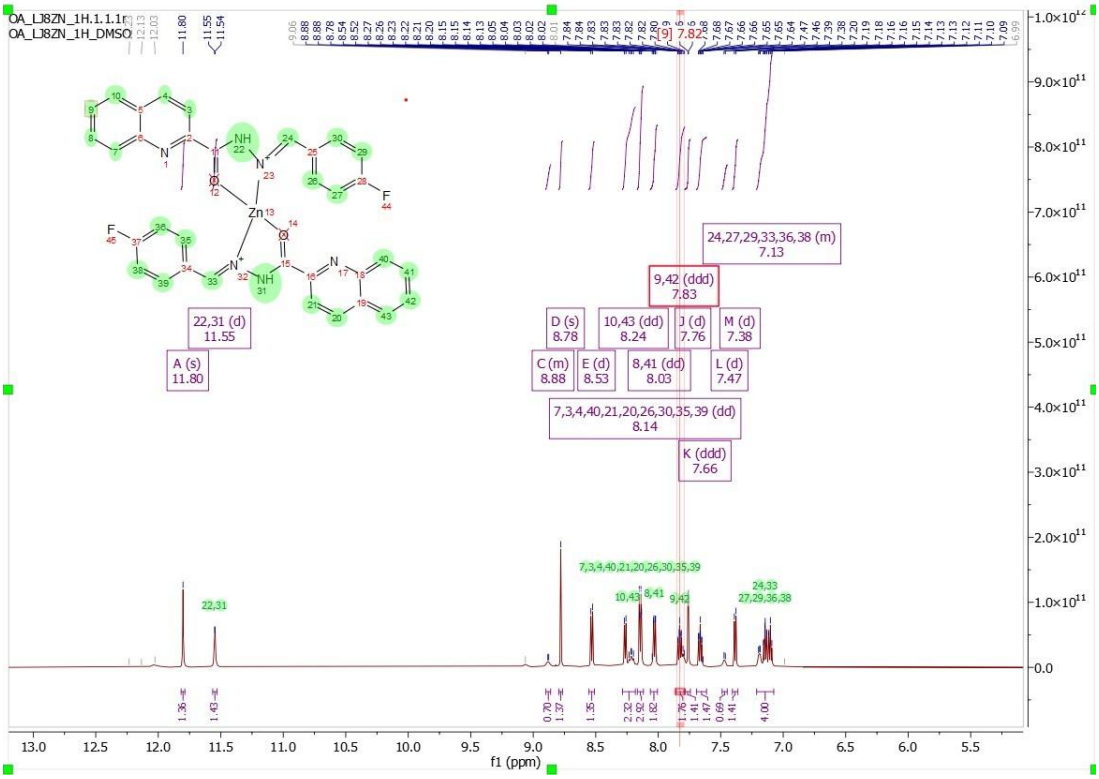

Fig. S17 ^{1}H NMR Spectrum of L4Zn

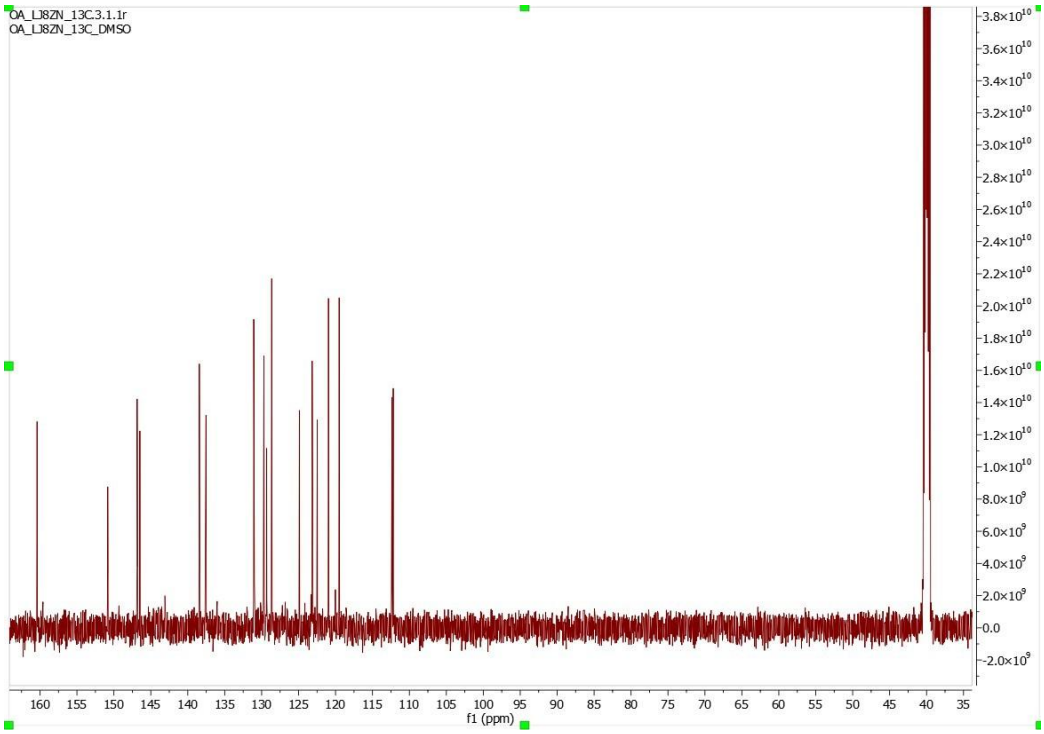

Fig. S18 ^{13}C NMR Spectrum of L4Zn

Mass Data

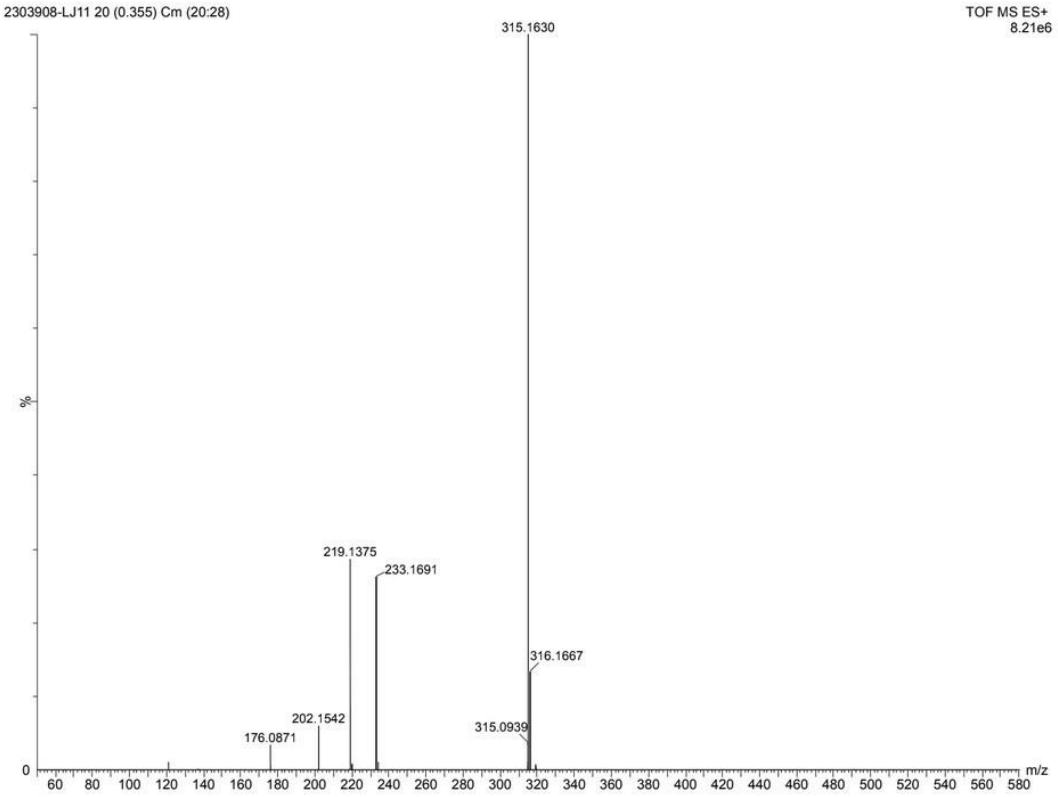

Fig. S19 ESI-MS Spectra of L3

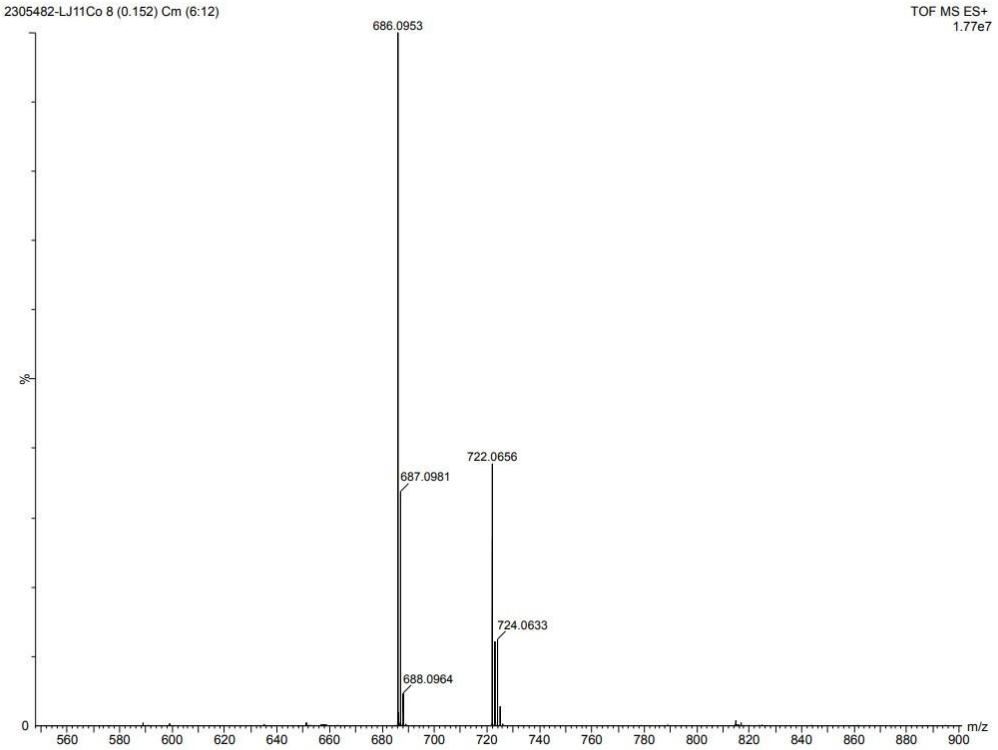

Fig. S20 ESI-MS Spectra of L3Co

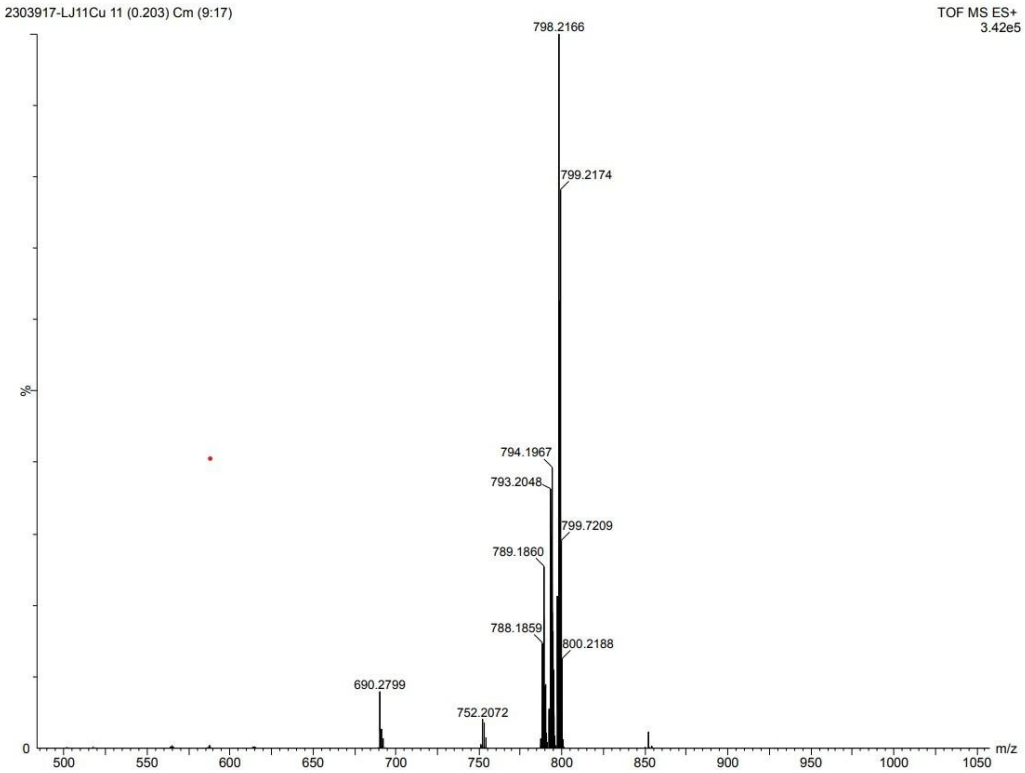

Fig. S21 ESI-MS Spectra of L3Cu

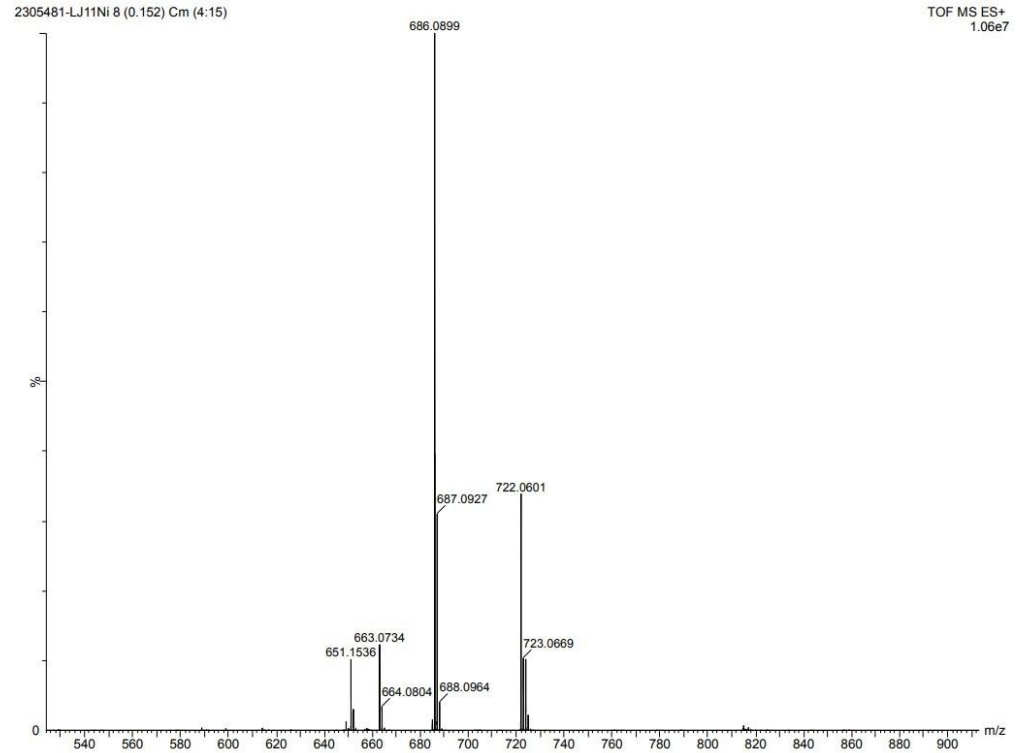

Fig. S22 ESI-MS Spectra of L3Ni

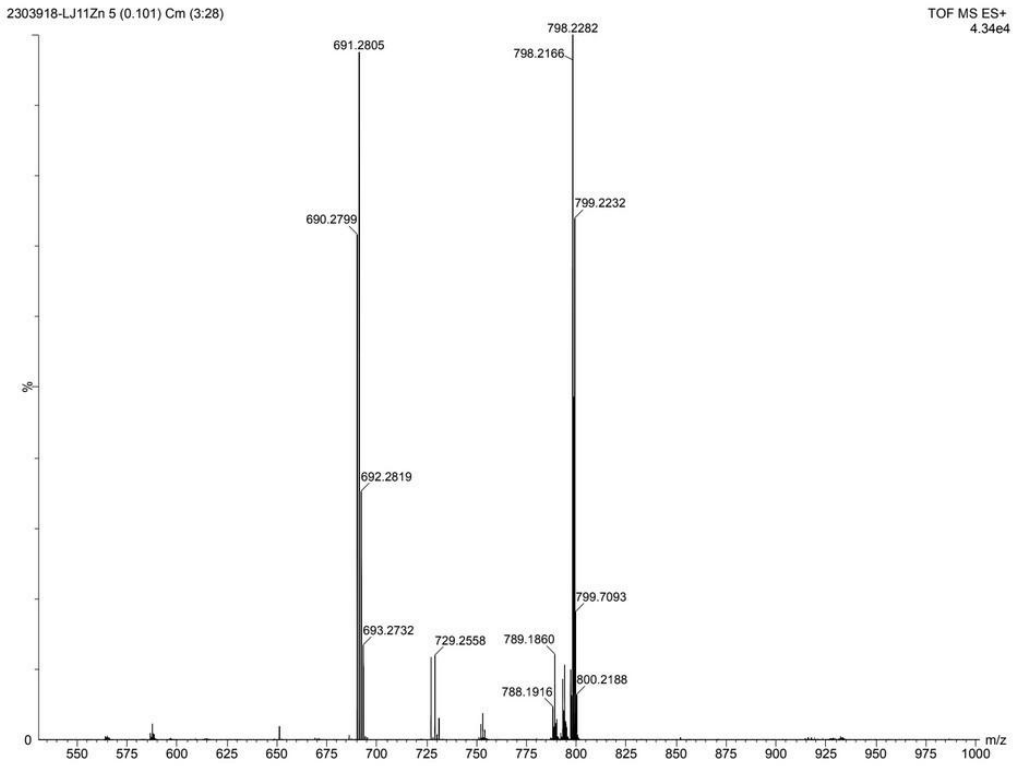

Fig. S23 ESI-MS Spectra of L3Zn

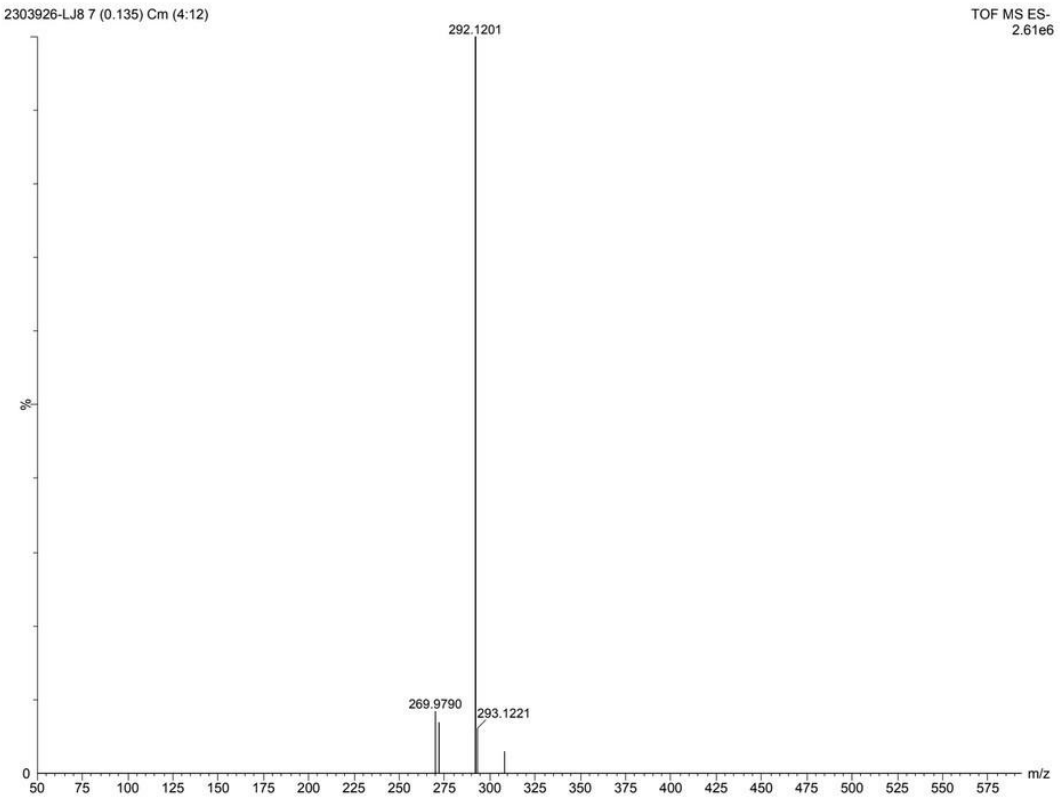

Fig. S24 ESI-MS Spectra of L4

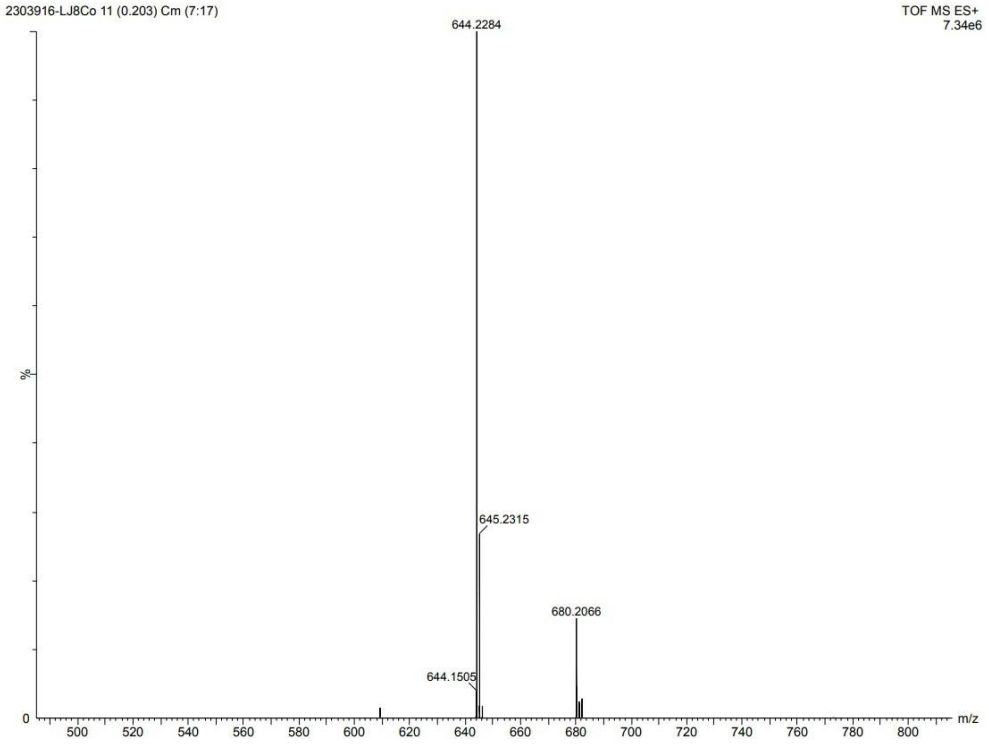

Fig. S25 ESI-MS Spectra of L4Co

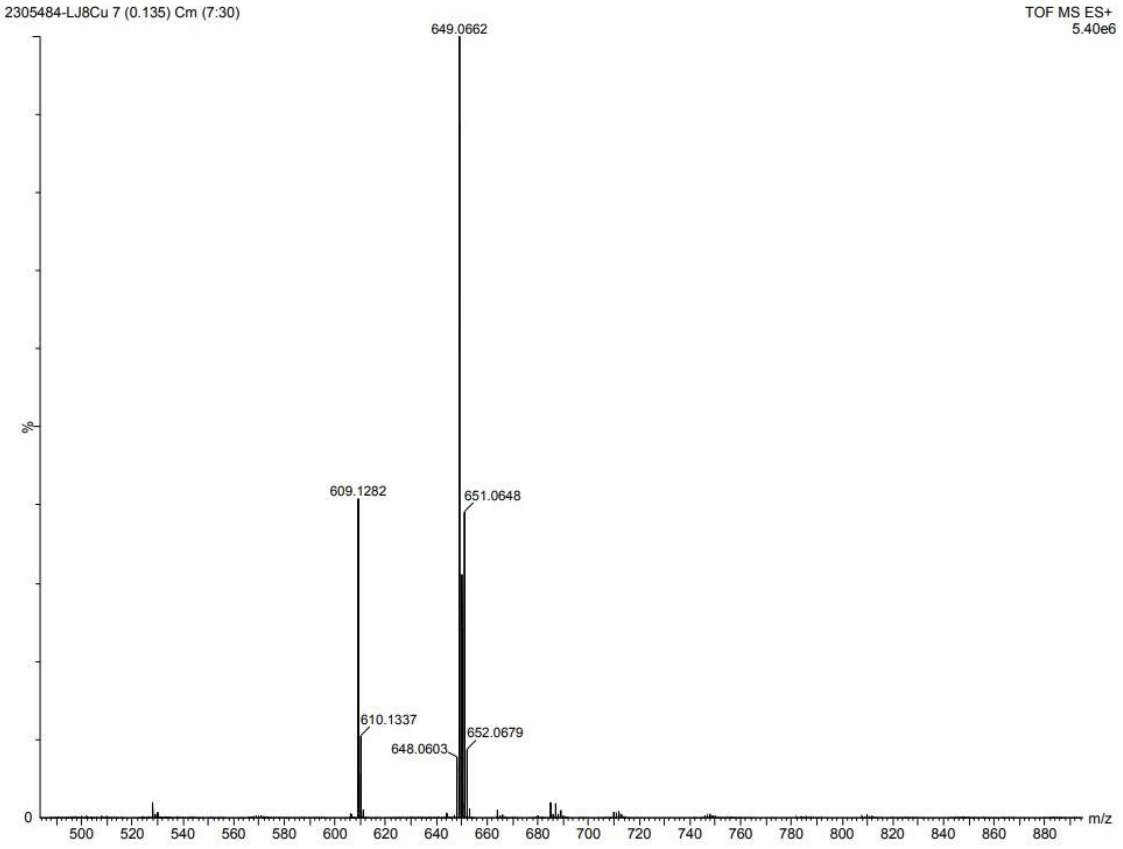

Fig. S26 ESI-MS Spectra of L4Cu

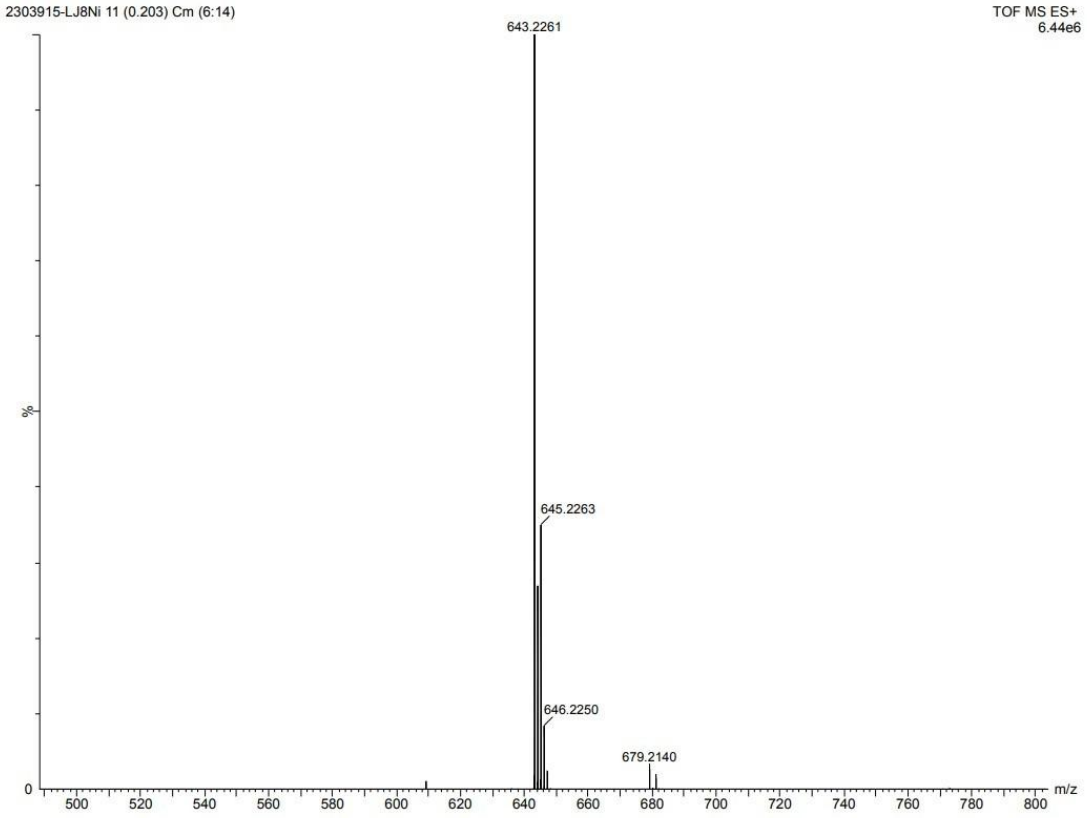

Fig. S27 ESI-MS Spectra of L4Ni

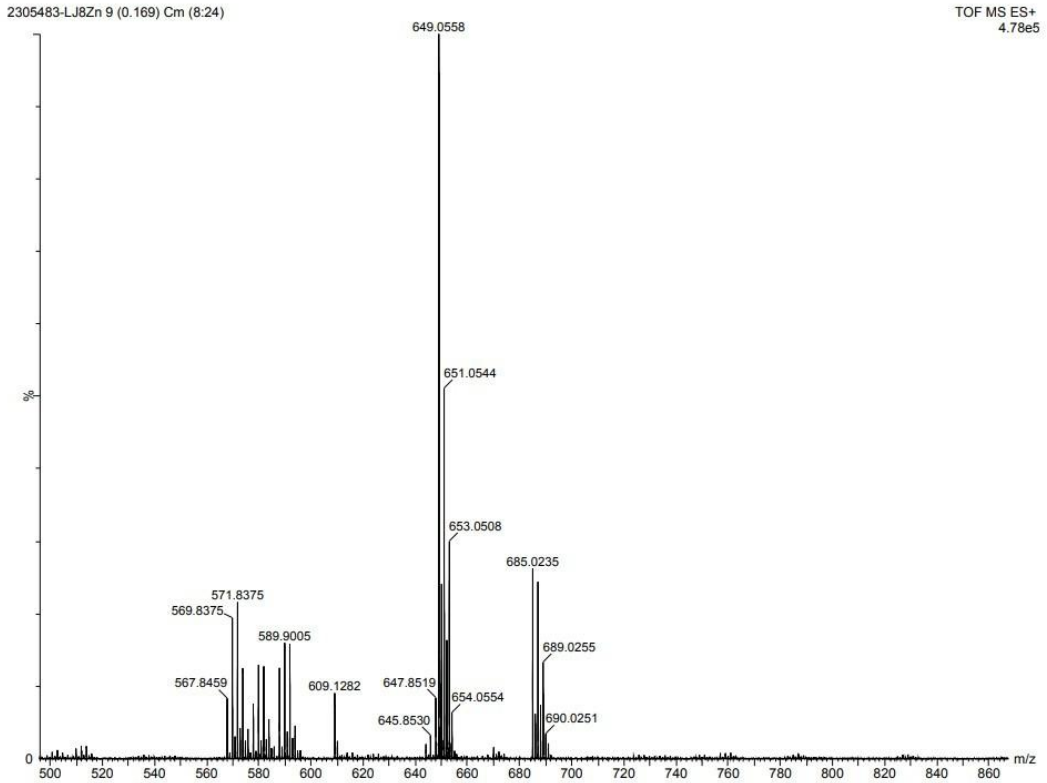

Fig. S28 ESI-MS Spectra of L4Zn

Anticancer Activity Results

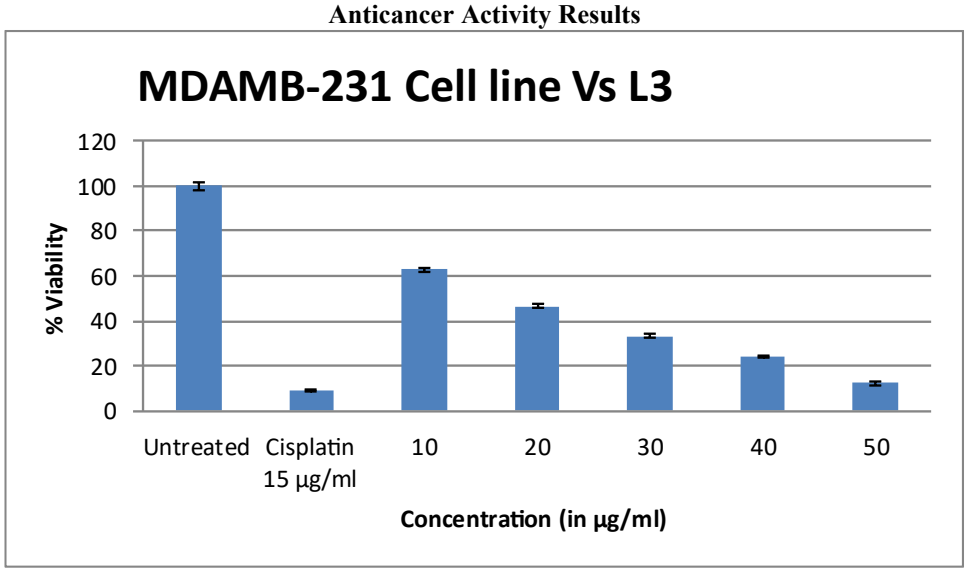

Fig. S29 *Percentage cell viability at various concentrations of L3*

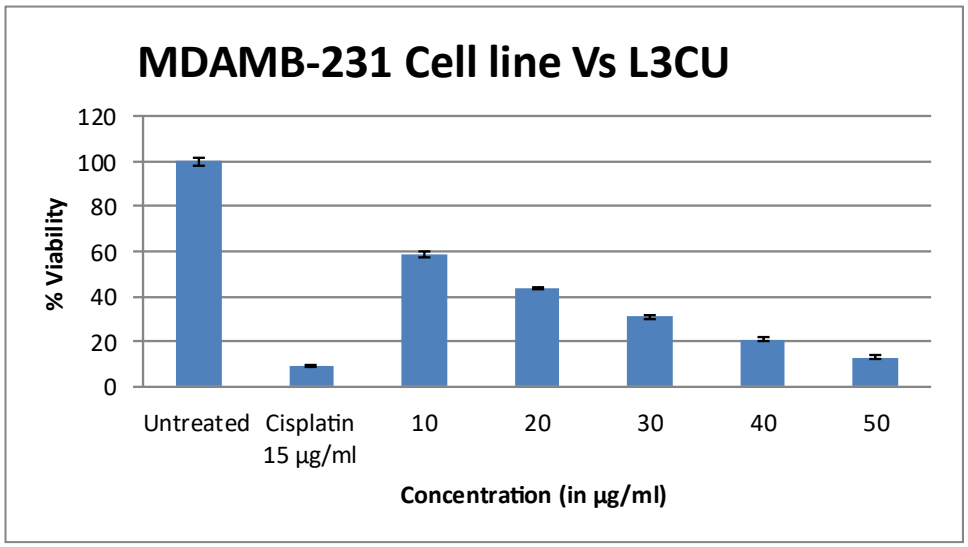

Fig. S30 *Percentage cell viability at various concentrations of L3Cu*

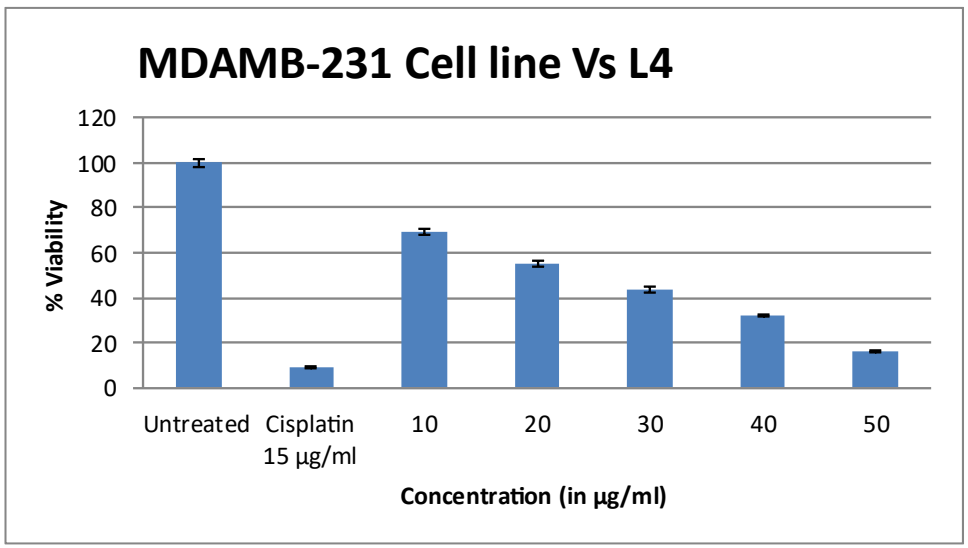

Fig. S31 *Percentage cell viability at various concentrations of L4*

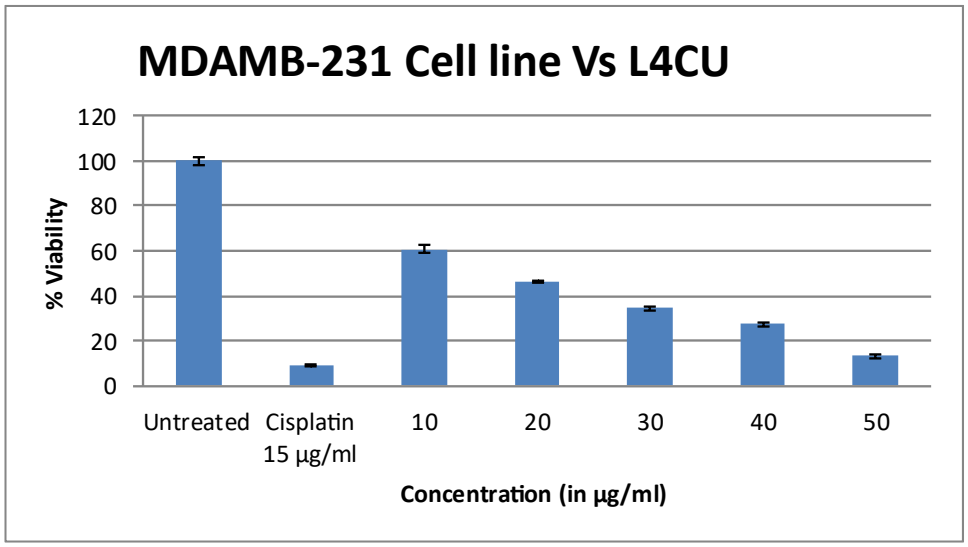

Fig. S32 *Percentage cell viability at various concentrations of L3Cu*

Table S1 Bond Angles of Ligand L3:

Number	Atom1	Atom2	Atom3	Angle
1	N1	O1	C4	117.3(2)
2	O1	N1	C3	118.3(2)
3	O1	N1	C14	122.3(2)
4	C3	N1	C14	119.3(2)
5	N3	N2	H6	118.4
6	H6	N2	C5	118.3
7	N3	N2	C5	123.3(2)
8	N2	N3	C6	112.8(2)
9	H1	C1	C2	119.4
10	H1	C1	C15	119.5
11	C2	C1	C15	121.1(2)
12	C1	C2	H14	119.7
13	C1	C2	C3	120.6(3)
14	H14	C2	C3	119.7
15	N1	C3	C2	119.6(2)
16	N1	C3	H13	120.2
17	C2	C3	H13	120.2
18	O1	C4	C5	117.8(2)
19	O1	C4	C12	124.3(2)
20	C12	C4	C5	117.9(2)
21	N4	C5	N2	125.6(2)
22	N2	C5	C4	114.4(2)
23	N4	C5	C4	120.0(2)
24	N3	C6	H7	118.2
25	C7	C6	N3	123.7(2)
26	C7	C6	H7	118.1
27	C8	C7	C6	131.4(2)
28	C19	C7	C6	123.0(2)

29	C19	C7	C8	105.6(2)
30	C9	C8	C7	107.1(2)
31	C16	C8	C7	133.9(2)
32	C9	C8	C16	118.9(2)
33	C8	C9	C10	122.6(2)
34	C8	C9	C18	107.7(2)
35	C10	C9	C18	129.7(3)
36	C9	C10	H10	121.2
37	C9	C10	C11	117.7(3)
38	H10	C10	C11	121.1
39	C10	C11	H2	119.1
40	C10	C11	C17	121.7(3)
41	C17	C11	H2	119.2
42	C4	C12	H5	120.6
43	C4	C12	C13	118.8(2)
44	H5	C12	C13	120.6
45	C12	C13	H3	120.2
46	C12	C13	C14	119.6(2)
47	H3	C13	C14	120.2
48	N1	C14	C13	117.7(2)
49	N1	C14	C15	118.7(2)
50	C13	C14	C15	123.5(2)
51	C1	C15	C14	120.6(2)
52	C1	C15	H4	119.7
53	C14	C15	H4	119.6
54	C8	C16	H12	121
55	C8	C16	C17	117.9(3)
56	H12	C16	C17	121.1
57	C11	C17	C16	121.1(3)
58	C11	C17	H11	119.4
59	C16	C17	H11	119.5
60	C9	C18	H9	125.6
61	C9	C18	C19	108.7(2)
62	H9	C18	C19	125.7
63	C7	C19	C18	110.9(3)
64	C7	C19	H8	124.6
65	C18	C19	H8	124.5

Table S2 All Torsions of Ligand L3

Number	Atom2	Atom3	Atom4	Torsion
1	O1	N1	C3	-177.2(2)
2	O1	N1	C14	1.4(3)
3	O1	C4	C5	-179.0(2)
4	O1	C4	C12	0.1(3)
5	N1	C3	C2	179.2(2)
6	N1	C3	H13	-0.8

7	N1	C3	C2	0.6(4)
8	N1	C3	H13	-179.4
9	N1	C14	C13	-1.2(3)
10	N1	C14	C15	179.3(2)
11	N1	C14	C13	177.3(2)
12	N1	C14	C15	-2.1(3)
13	N2	N3	C6	9.5
14	N2	N3	C6	-170.4(2)
15	N2	C5	N4	176.1
16	N2	C5	C4	-6.1
17	N2	C5	N4	-4.0(4)
18	N2	C5	C4	173.8(2)
19	N3	C6	H7	-1
20	N3	C6	C7	179.0(2)
21	C1	C2	H14	-1.1
22	C1	C2	C3	178.9
23	C1	C2	H14	179
24	C1	C2	C3	-1.0(4)
25	C1	C15	C14	179.5
26	C1	C15	H4	-0.4
27	C1	C15	C14	-0.5(4)
28	C1	C15	H4	179.6
29	C2	C3	N1	1.0(4)
30	C2	C3	H13	-179
31	C2	C3	N1	-179
32	C2	C3	H13	1
33	C4	C5	N2	13.8(3)
34	C4	C5	N4	-168.3(2)
35	C4	C5	N2	-165.3(2)
36	C4	C5	N4	12.6(3)
37	C4	C12	H5	178.4
38	C4	C12	C13	-1.6(4)
39	C4	C12	H5	-2.6
40	C4	C12	C13	177.5(2)
41	C6	C7	C8	-4.7(4)
42	C6	C7	C19	176.3(3)
43	C6	C7	C8	175.3
44	C6	C7	C19	-3.7
45	C7	C8	C9	-179.3(3)
46	C7	C8	C16	-3.6(5)
47	C7	C8	C9	-0.2(3)
48	C7	C8	C16	175.5(3)
49	C7	C19	C18	179.4(2)
50	C7	C19	H8	-0.6
51	C7	C19	C18	0.1(3)
52	C7	C19	H8	-179.8

53	C8	C9	C10	178.8(3)
54	C8	C9	C18	0.2(3)
55	C8	C9	C10	2.3(4)
56	C8	C9	C18	-176.3(2)
57	C8	C16	H12	3.9
58	C8	C16	C17	-176.1(3)
59	C8	C16	H12	179.2
60	C8	C16	C17	-0.7(4)
61	C9	C10	H10	177.9
62	C9	C10	C11	-2.0(4)
63	C9	C10	H10	-3.9
64	C9	C10	C11	176.2(3)
65	C9	C18	H9	179.9
66	C9	C18	C19	-0.1(3)
67	C9	C18	H9	1.4
68	C9	C18	C19	-178.6(3)
69	C10	C11	H2	-179.7
70	C10	C11	C17	0.3(5)
71	C10	C11	H2	0.4
72	C10	C11	C17	-179.6
73	C11	C17	C16	1.2(5)
74	C11	C17	H11	-178.7
75	C11	C17	C16	-178.8
76	C11	C17	H11	1.2
77	C12	C13	H3	-178.4
78	C12	C13	C14	1.6(4)
79	C12	C13	H3	1.6
80	C12	C13	C14	-178.3
81	C13	C14	N1	-0.3(3)
82	C13	C14	C15	179.1(2)
83	C13	C14	N1	179.7
84	C13	C14	C15	-0.9
85	C14	C15	C1	2.1(4)
86	C14	C15	H4	-178
87	C14	C15	C1	-177.3(2)
88	C14	C15	H4	2.6
89	C16	C17	C11	-1.0(5)
90	C16	C17	H11	179
91	C16	C17	C11	179.1
92	C16	C17	H11	-0.9
93	C18	C19	C7	-0.0(3)
94	C18	C19	H8	179.9
95	C18	C19	C7	180
96	C18	C19	H8	-0.1